Geophysica (2024), 59 (1), 21–52

Site Characterization of Muzaffargarh Region, Pakistan, using HVSR Analysis of Seismic Events and Ambient Noise Data

Azmat Azad[1,*], *Muhammad Tahir*[1], *Bilal Saif*[1], *Talat Iqbal*[1], *and Muhammad Ali Shah*[1]

[1]Centre for Earthquake Studies, National Centre for Physics, Islamabad, Pakistan
[*]Corresponding mail address, azmat_azad@hotmail.com

(Submitted: 2024-05-29; Accepted: 2024-12-10)

Abstract

The Muzaffargarh region's Horizontal-to-Vertical Spectral Ratio (HVSR) is performed using ambient noise and three seismic events from local to teleseismic distances. Local site parameters such as the fundamental frequencies of the soft soil layer above bedrock and peak amplitudes of corresponding HVSR are estimated. The average fundamental frequency of the site based on earthquake data using five stations installed at Muzaffargarh (thick sediments) is $1.2\,\mathrm{Hz}$*, while higher fundamental site frequency (*$3.67\,\mathrm{Hz}$*) is observed at another station that is installed on hard rock in a nearby location. Similar results of HVSR are validated by using ambient noise data recorded by these stations. Relatively low frequency fundamental site frequency peak (*$\sim 1\,\mathrm{Hz}$*) of seismic motion is associated with the existence of homogenous sedimentary cover (*$\sim 60\,\mathrm{m}$*) in the area. Seismic vulnerability index (*6.72 *to* 9.63*) is also calculated from fundamental site frequency and amplitude values for quantification of seismic hazard potential in the study area. These local soil conditions play a vital role in evaluation of the seismic response of structures, seismic hazard assessment and earthquake risk mitigation. Similarly, site effects estimation is an important procedure for highlighting frequencies of subsurface shallow layers and to ensure that they are not critically close to natural frequencies of buildings in the area.*

Keywords: HVSR; Muzaffargarh; ambient noise; earthquake; fundamental frequency; vulnerability index

1 Introduction

The loose sediments amplify seismic ground motion during an earthquake and cause severe damage to buildings (*Edwards*, 2006; *Guillier et al.*, 2014). Apart from destruction caused by the magnitude of earthquake (which quantifies the energy released) and distance from the epicenter, several cities in the past have experienced damage due to amplified ground motion due to local site conditions (*Fat-Helbary et al.*, 2019). Examples include Mexico 1985, Cairo 1992, Northridge 1994, Kobe 1995, Quindio 1999, Kocaeli 1999, Athens 1999, Bhuj 2001, Bam 2003, Sumatra 2004, and Haiti 2010 earthquakes that produced damages to cities constructed on soft sediments (*Goda et al.*, 2018). These examples describe that seismic waves are entrapped and amplified in soft sediments as compared to bedrock. Moreover, geometric features of the deposit, physical properties of the terrains and frequency content of the seismic waves all contribute to interference (*Panzera et al.*, 2013). The earthquake behavior is a complex process and is a result of the interplay between the earthquake source, the propagation path of seismic waves, and the site conditions at the surface. Each of these factors plays a vital role in determining the intensity, duration, and impact of the shaking at a given site. Earthquake sources involve the nature of the movement, depth, and magnitude. Shallow-focus earthquakes cause more intense ground shaking at the surface compared to deep-focus earthquakes of same magnitude (*Kanamori*, 1977). Similarly, a large earthquake tends to produce stronger shaking and propagate seismic waves over greater distances (*Boore*, 2003). Seismic waves typically lose energy as they travel through the Earth, and attenuation increases with distance. Earth's geological structure and composition affect how seismic waves propagate, i.e., the path can either amplify or reduce wave energy (*Aki and Richards*, 2002). It is observed that areas underlain by soft soils experience greater shaking of ground motion compared to those located on bedrock (*Cakir and Walsh*, 2012). The process that involves the impact of underlying soil on local amplification of earthquake shaking is called site effect, which is an important consideration in modern seismic hazard assessments (*Theilen-Willige*, 2010). The horizontal subsurface layers of the Earth, especially those with varying compositions and thicknesses, have the potential to trap seismic body waves which move through the Earth's interior in a vertical motion (up and down). This phenomenon occurs due to velocity contrasts between different layers, where seismic waves encounter boundaries with abrupt changes in material properties, like soft sediments overlying hard rock. These contrasts lead to the reflection and refraction of seismic waves, causing them to become confined within certain layers (*Bouchon*, 1981). Likewise, the lateral variations in the soil composition or layer thickness further contribute to this effect, especially when the seismic waves encounter heterogeneous structures. In such environments, surface waves are particularly susceptible to trapping, as they move along the Earth's surface. When trapped, these waves can interfere with each other, both constructively and destructively, leading to resonance patterns. This resonance can significantly amplify the seismic waves, enhancing the ground motion in certain frequencies, which is often seen in areas with soft soils or sedimentary layers (*Frankel*, 1993). These effects can cause severe shaking during an earthquake, especially if the natural frequency of the surface layer aligns with the frequency of the seismic waves, amplifying the destructive potential of ground motions (*Field and Jacob*, 1993; *Lermo and Chávez-García*, 1994; *Bonilla et al.*, 1997; *Bour et al.*, 1998; *Bard*, 1998; *Woolery and Street*, 2002; *Molnar and Cassidy*, 2006; *Haghshenas et al.*, 2008; *Fäh et al.*, 2009; *Fat-Helbary et al.*, 2019). The mechanical and geometrical properties of the layers have an influence on the fundamental site frequency (*Panzera et al.*, 2012). Resonance phenomenon occurs when the fundamental frequency of the foundation soil matches the natural frequency of the building that increases a chance of collapsing (*Mukhopadhyay and Bormann*, 2004). This emphasizes the importance of site effects in the design of new constructions, retrofitting of existing structures, and prior land use planning for building construction (*Haghshenas et al.*, 2008). Although, it is possible to determine site characterization through drilling but it is an expensive, time consuming and difficult to perform in urban areas. However, fundamental site frequencies, amplification factor, and V_{S30} (shear wave velocity at 30 m depth) profiles obtained by analysis of earthquakes, ambient noise or microtremors provide a convenient alternate way of finding shallow subsurface structures. The shallow and near surface velocity profile is crucial because it directly affects how seismic waves propagate through the Earth's crust and the level of ground shaking that can be expected at the surface during an earthquake. It is useful in seismic hazard assessment (*Bindi et al.*, 2011), seismic site response analysis (*Zhao et al.*, 2006), building design and structural engineering (H. *Seed and Idriss*, 1970), soil liquefaction potential (*Stokoe et al.*, 2001), and seismic microzonation (*Gomberg et al.*, 2005). The HVSR technique is a low cost and reliable substitute for drilling and active seismic survey (*Kawase et al.*, 2011; *Garofalo et al.*, 2016; *Kang et al.*, 2020a).

The Horizontal to Vertical Spectral Ratio (HVSR) technique is widely used to determine the fundamental site frequency and has proven an efficient and robust tool for site evaluation (*Bonnefoy-Claudet et al.*, 2006; *Kawase et al.*, 2011; *Lunedei and Malischewsky*, 2015; *Gupta et al.*, 2018, 2019, 2021). This technique produces a distinct peak at the fundamental frequency in soft sediments which reflects the impedance contrast between the top layer of soil and the basement rock (*Kang et al.*, 2020a). The HVSR spectra produced for any site can further be used for calculation of shear wave velocity (V_{S30}) through velocity inversion (*Kawase et al.*, 2011; *Haryono et al.*, 2020). Moreover, microzonation of cities such as; Quito, Almeria, Barcelona and Caracas were also carried out by this technique (*Guéguen et al.*, 2000; *Alfaro et al.*, 2002; *Navarro et al.*, 2002).

In this research, HVSR technique is used to study Muzaffargarh region (Figure 1.1), located in southern part of Punjab province (Pakistan). The region is part of Sulaiman Foredeep, formed due to deposition of Indus River. The basement is composed of consolidated igneous or metamorphic rocks, overlain by thick loose sedimentary layers (*Kazmi and Jan*, 1997). Mainly, the Sulaiman fold and thrust belt present to west of the area contributes small to moderate size seismicity in this region (*Ahmed and Ghazi*, 2022). Teleseismic ($> 30°$) to local ($< 10°$) earthquakes and ambient noise data are utilized (Table 1.1) for H/V ratio calculation. The values of fundamental site frequency and amplitude obtained from HVSR method are then utilized for calculation of seismic vulnerability index (K_g). K_g represents the vulnerability of ground surface and buildings to earthquake motion (*Abd El-Aal*, 2010; *Liu et al.*, 2014). Large K_g values are representative of weak points and hence most vulnerable locations. Recently, a number of critical structures and different economic projects are ongoing in this area but a comprehesive study regarding the quantification and existence of soft soil is lacking in the literature. Therefore, we considered five seismic stations, installed since 2019 in the area, for HVSR calculation. These results are further compared and confirmed with a station installed on hard rock.

2 *Tectonic and Geological Settings*

Three major tectonic plates, i.e., Indian, Eurasian and Arabian are present in the proximity of Pakistan (Figure 2.1) that caused some parts to be seismically active regions of the world (*Stein et al.*, 2002; *Copley et al.*, 2010). The Indian plate is drifting northward, colliding with the Eurasian plate at rate of $20\,\mathrm{mm\,yr^{-1}}$ whereas its western boundary is converging obliquely with Eurasian plate at a double slip rate (approximately $42\,\mathrm{mm\,yr^{-1}}$) and rotating anticlockwise (*DeMets et al.*, 1990; *Gripp and Gordon*, 1990; *Aitchison et al.*,

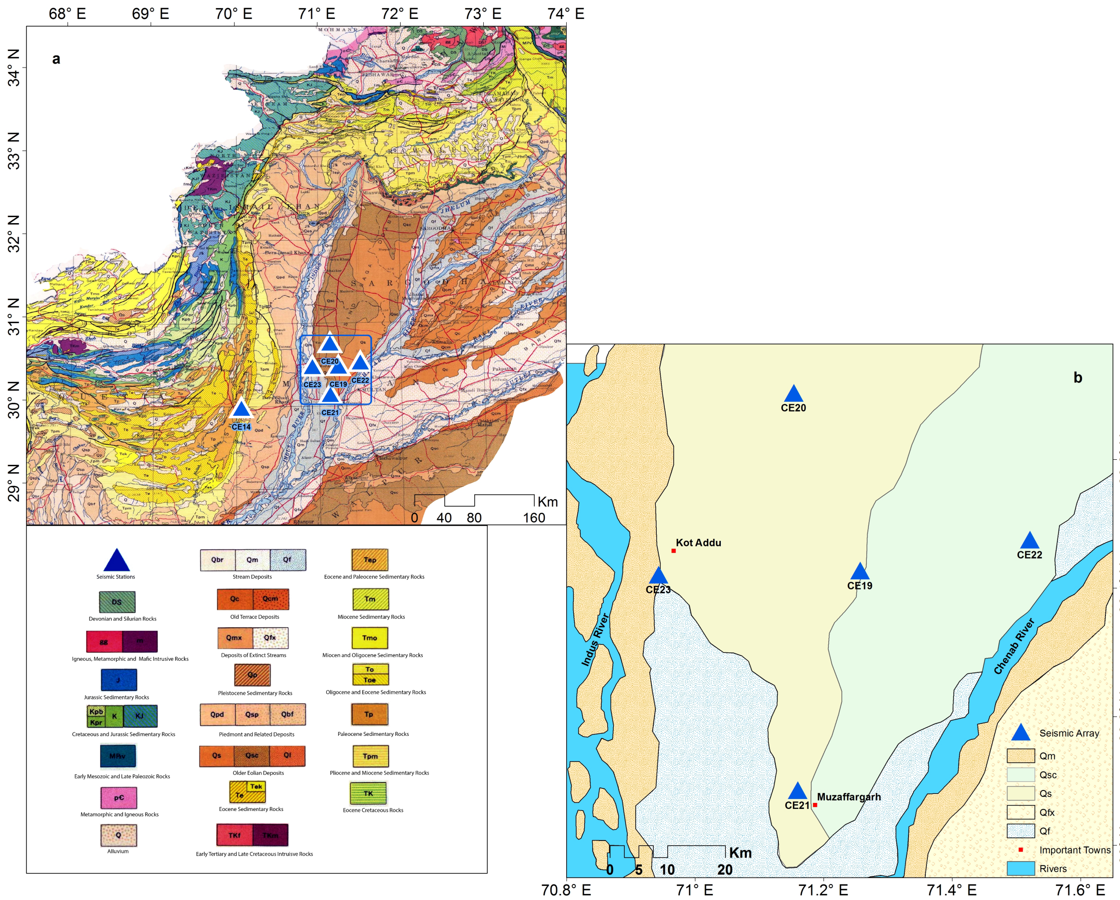

Fig. 1.1: Map showing location and geology of the study area as well as distribution of the seismic stations considered in the study. Detailed geology of the region (*Pakistan*, 1964) with station location is shown sub-figure a while sub-figure b represents the geology of the study area alongwith the location of 5 seismic stations installed in this region and important towns. Qm: Streambed and meander-belt deposits, Qsc: Barchan, sayf or complex dunes; relief less than 100 feet. Eolian sand deposits, deposits of extinct streams, Qs: Eolian Sand, Qfx: Flood-plain deposits (lower terrace), Qf: Flood-plain deposits. The deposits shown in sub-figure b belongs to quaternary age group (modified from Geological Survey of Pakistan map, 1964. Scale 1 : 2 000 000)

2007). The western border of Pakistan is therefore, marked by transform plate boundary between these two plates. This has resulted in formation of left-lateral transform slip in Baluchistan which comprises of the Chaman and Ornach Nal Fault Zones (*O'Brien et al.*, 2001; M. *Khan et al.*, 2008). To the south, Arabian plate is subducting beneath the Eurasian plate at rate of 23 mm yr^{-1}. This process has resulted in creation of the Makran Subduction Zone (*Treloar and Izatt*, 1993). A series of fold and thrust belts of Sulaiman and Kirthar Ranges, which are the south-western extension of Himalayan mountain belt, are also present here (*Bender and Raza*, 1995; *Kazmi and Jan*, 1997). The eastern and southern boundaries of the Sulaiman Range are marked by broad folds abutting alluvial deposits of the Indus river system, which flows through the active Himalayan foredeep (*Humayon*, 1990).

The study area is located in Central Indus Basin (Figure A.1), which can be subdivided into three physiographic units. These include Punjab Platform, Sulaiman Fore-

Table 1.1: List of seismic events recorded at Muzaffargarh array

S. No	Date	HH:MM:SS	Lat.	Long.	Depth (km)	Mag.	Average Distance from Epi-center	Region
1	07/02/2021	05:46:10.1	−2.830	144.390	50	6.3 M_b	8724 km	Papua New Guinea
2	21/06/2022	20:54:35.5	32.945	69.474	10	5.9 M_l	333 km	Pak–Afghan Border
3	29/06/2022	04:30:32.7	36.248	70.699	223	5.2 M_l	654 km	Hindu Kush, Afghanistan

deep/Depression and Sulaiman Foldbelt while moving from east to west. Indian Shield marks the eastern boundary of Central Indus Basin while the western side is bounded by marginal zone of Indian Plate. Sargodha high and Pezu rift are located in north whereas the Sukkur rift is present in the south. The Punjab platform is covered by thick alluvium comprising of clay, silt, and sand layers (*Khalid et al.*, 2014). The Sulaiman Foredeep (which is part of Central Indus Basin and where study area is located) is a large area of subsidence that becomes arcuate along its southern edge and takes up a transverse orientation. The eastern and southern parts of Sulaiman Foredeep are marked by low, barren hills composed of alluvium and post-Eocene fluviatile clastics (Clastic fluvial material) which ultimately merges with Punjab Platform. The northern and western parts of the depression show high relief with rock outcrops of Tertiary carbonates and shale. The exposed rocks in these parts form an orographically uplifted area (*Raza et al.*, 1989). Duplex structures are common in the Sulaiman fold and thrust belt, which contribute actively in producing seismicity in this region (*Reynolds et al.*, 2015). Quetta–Sibi syntaxis in the northwest of the site is one example of such active fold and thrust belt (*Wandrey et al.*, 2004). According to various authors, left and right lateral transpressional regimes related to wrench tectonics in the east and west developed the Suleiman Fold Belt during late Tertiary (*Kazmi and Jan*, 1997; *Bernard et al.*, 2000; *Reynolds et al.*, 2015). Wrench-related tectonics has been observed on the surface. The left-lateral en-echelon folds and associated thrust faults in the east and right-lateral en-echelon folds and related fault systems in the west are some examples of these wrench tectonics (Figure 2.1). The existence of thick sedimentary cover (10 km to 15 km) in foredeep zone is reported in previous studies (*Raza et al.*, 1989, 1990). Structurally the sedimentary cover of foredeep is comprised of several large, gently dipping anticlinal flexures and fault blocks (*Kazmi and Jan*, 1997).

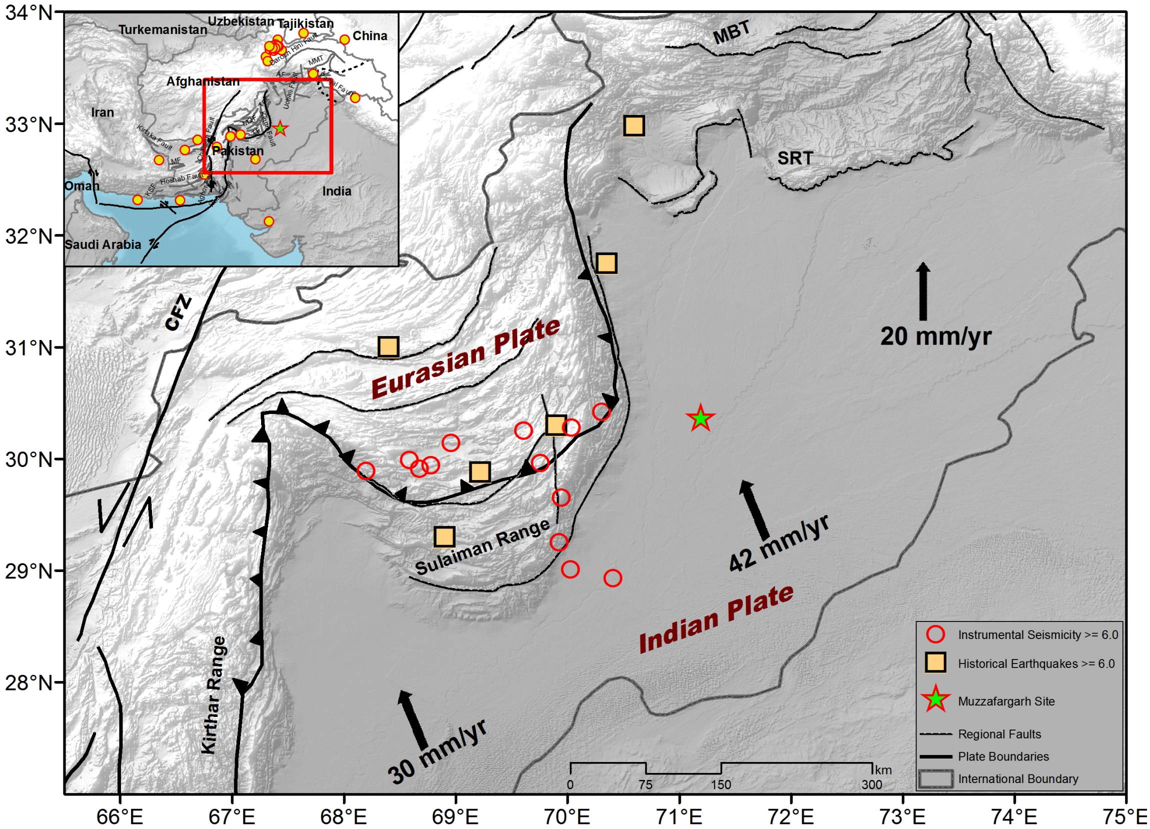

Fig. 2.1: Tectonic settings of the study area (main figure) showing plate boundary between Indian and Eurasian plates and major seismogenic structures of the region. MBT: Main Boundary Thrust, SRT: Salt Range Thrust, CFZ: Chamman Transform Fault Zone, Sulaiman range and Kirthar Range. Major historical earthquakes are shown by squares and instrumental seismicity is indicated by circles. Tectonic plate boundaries are marked by thick black lines. Black arrows show the convergence vector of Indian plate relative to Eurasian Plate. Top left subfigure shows the regional tectonic settings of Pakistan and Arabian, Eurasian and Indian plates along with their movement direction and rate. The red rectangle represents the area under study.

3 *Materials*

Seismic data from Centre for Earthquake Studies (CES) are used in this study. CES has deployed five stations around the Muzaffargarh region to detect and monitor seismicity. These stations are equipped with broadband seismometers (Guralp CMG-3T), working in continuous mode. The digitizer, DM24 with six channels, is mounted on these stations. The sampling frequency rate is 50 samples per second, with GPS time synchronization available on these stations. These seismic sensors are duly coupled with ground and installed on a small concrete platform within a vault. Essential accessories, such as batteries and transmitters, are housed in adjacent room. All stations are powered by electric solar panel system and transmit data via satellite link to the CES Islamabad.

Both, earthquakes and seismic noise data, recorded during 1st January 2021 to 31st July 2022 are used for HVSR measurements. The events have variable depths (shallow, 10 km and deep, 223 km) and magnitude between 5.2 m_l to 6.7 m_b. The selected earthquake data (Table 1.1) quality were tested against different parameters (like length of recorded data, number of windows, fundamental site frequency, amplitude etc.) for analysis. The data include events from local ($< 10°$) to teleseismic ($> 30°$) distances and only those events that are recorded on maximum number of stations of the Muzaffargarh region are selected.

Additionally, ambient noise data of day time (10:00 AM to 11:00 AM) and night time (10:00 PM to 11:00 PM) for the same stations are also used. Those sites having lower fundamental frequencies, one hour or more than hour longer data recording is required. This ensures that enough time windows are available to carry out reliable data processing (*Molnar et al.*, 2021). Therefore, one-hour long noise waveform data were selected for each of these stations as they have low fundamental frequencies with the exception of CE14 station because it is installed on hard-rock and has high fundamental frequency.

4 Data Processing and Interpretation

Data viewing and processing are performed with SCREAM and SEISAN (*Havskov et al.*, 2020) software respectively. For HVSR calculation at any particular station GEOPSY (*Wathelet et al.*, 2020), an open-source software, is used by following **S**ite **E**ffect**S** assessment using **AM**bient **E**xcitations (SESAME2004) guidelines as shown in Table 4.1. GEOPSY calculates the average spectra of the two horizontal components and the vertical component and then determine the ratio of the horizontal and vertical amplitude spectra. The output produces a prominent peak at the fundamental site frequency. For data processing of seismic events (following the recommendations of SESAME) window size is optimized according to the length of the recorded event i.e. starting from onset of P-waves up to the coda (Table 4.2). A sixty second window length is used for ambient noise analysis (Table 4.3). However, selection of a different value of window length (as long as the condition, $f_0 > 10/l_{\mathrm{w}}$ is fulfilled) does not disturb the shape of the spectra. Sudden and unexpected discontinuities can affect the Fourier Spectrum therefore, Cosine taper of 5% is applied at both ends of the selected data window to resolve this problem (*Chatelain and Guillier*, 2013). The horizontal and vertical Fourier amplitude spectra is smoothed by applying Konno–Ohmachi algorithm. In case of noise data Short Term Average (STA) and Long Term Average (LTA) are used to remove transient effects in each data time window. STA and LTA window lengths are set at 2 s and 5 s, respectively. Minimum value of STA/LTA is 0.2% while maximum value is 2.5%.

We used the peak fundamental site frequency and amplitude values for calculation of seismic vulnerability index (K_{g}) at each site using; $K_{\mathrm{g}} = A^2/f_0$, where A is the amplification factor and f_0 is the fundamental site frequency obtained from HVSR (*Nakamura*, 1997; *Liu et al.*, 2014). Higher K_{g} value is observed at thick soil layer as compared to hard rock site and is used for calculating the damage possibility prior the earthquake occurrence (*Beroya et al.*, 2009; *Warnana et al.*, 2011; *Adib et al.*, 2015; *Sugianto et al.*, 2016). This is an important engineering term used for seismic microzonation and buildings assessment. Buildings in regions of higher K_{g} value might require retrofitting. Finally, we examined the impact of distance and depth of the seismic events on fundamental site frequency. The

Table 4.1: Criteria for a reliable H/V curve and clear H/V peak

Criteria	
$f_0 > \frac{10}{l_\mathrm{w}}$ $n_\mathrm{c} \cdot f_0 > 200$ $\sigma_A(f) < 2$ for $0.5f_0 < f < 2f_0$ if $f_0 > 0.5$ Hz, or $\sigma_A(f) < 3$ for $0.5f_0 < f < 2f_0$ if $f_0 < 0.5$ Hz $\exists f^- \in [f_0/4, f_0] \mid A_\mathrm{HV}(f^-) < A_0/2$ $\exists f^+ \in [f_0, 4f_0] \mid A_\mathrm{HV}(f^+) < A_0/2$ $A_0 > 2$ $f_\mathrm{peak}[A_\mathrm{HV}(f) \pm \sigma_A(f)] = f_0 \pm 5\%$ $\sigma_f < \varepsilon(f_0)$ $\sigma_A(f_0) < \Theta(f_0)$	Where: • l_w: Length of window (seconds). • n_c: Number of cycles. • f: Current frequency (Hz). • f_0: Fundamental site frequency (Hz). • $\sigma_A(f)$: "Standard deviation" of $A_{HV}(f)$, the factor by which the mean $A_{HV}(f)$ curve should be multiplied or divided. • $A_\mathrm{HV}(f)$: H/V curve amplitude at frequency f. • f^-: Frequency between $f_0/4$ and f_0 for which $A_\mathrm{HV}(f) < A_0/2$. • f^+: Frequency between f_0 and $4f_0$ for which $A_\mathrm{HV}(f^+) < A_0/2$. • A_0: H/V peak amplitude at frequency f_0. • f_peak: Peak frequency. • $\sigma_A(f)$: Same as above. • σ_f: Standard deviation of H/V peak frequency. • $\varepsilon(f_0)$: Threshold value for the stability condition. • $\Theta(f_0)$: Threshold value for stability condition $\sigma_A(f_0) < \Theta(f_0)$.

polarization and occurrence of distinct phases within seismic sources are greatly impacted by the distance and depth from the source to the receiver.

5 Results

The fundamental frequencies of five sites in Muzaffargarh region are estimated using earthquakes (Table 4.2) and ambient noise data (Table 4.3) recorded on five seismic

Table 4.2: Earthquake details and processing parameters for HVSR calculation of Muzaffargarh array and CE14 station.

Station	Date	$^{1}n_{\mathrm{w}}$	$^{2}l_{\mathrm{w}}$	$^{3}f_0$	$^{4}A_0 > 2$	$^{5}n_{\mathrm{c}} = n_{\mathrm{w}} \cdot l_{\mathrm{w}}$	$f_0 \geq 10/l_{\mathrm{w}}$	$n_c \cdot (f_0) > 200$	Remarks	Lat.	Long.	Depth	Mag.	Region
CE19	07/02/2021	11	50	1.10	2.71	550	0.2	605.00	Reliable	−2.830	144.390	50.00	6.3 M_b	Papua New Guinea
	21/06/2022	13	30	1.22	2.59	240	0.5	292.80	Reliable	32.945	69.474	10.00	5.9 M_l	Pak–Afghan Border
	29/06/2022	12	50	1.31	2.94	600	0.2	786.00	Reliable	36.248	70.699	223.0	5.2 M_l	Hindu Kush, Afghanistan
CE20	07/02/2021	11	50	1.12	2.54	550	0.2	616.00	Reliable	−2.830	144.390	50.00	6.3 M_b	Papua New Guinea
	27/06/2022	12	20	1.22	2.59	240	0.5	292.80	Reliable	32.945	69.474	10.00	5.9 M_l	Pak–Afghan Border
	29/06/2022	12	50	1.32	2.64	600	0.2	792.00	Reliable	36.248	70.699	223.0	5.2 M_l	Hindu Kush, Afghanistan
CE21	07/02/2021					*(No data)*			**Station Offline**					
	27/06/2022	12	20	1.28	2.21	240	0.5	307.20	Reliable	32.945	69.474	10.00	5.9 M_l	Pak–Afghan Border
	29/06/2022	12	50	1.17	2.12	600	0.2	702.00	Reliable	36.248	70.699	223.0	5.2 M_l	Hindu Kush, Afghanistan
CE22	07/02/2021					*(No data)*			**Station Offline**					
	27/06/2022	12	20	1.46	2.60	240	0.5	350.40	Reliable	32.945	69.474	10.00	5.9 M_l	Pak–Afghan Border
	29/06/2022	15	50	1.26	2.43	750	0.2	945.00	Reliable	36.248	70.699	223.0	5.2 M_l	Hindu Kush, Afghanistan
CE23	07/02/2021	11	50	1.05	2.75	550	0.2	577.50	Reliable	−2.830	144.390	50.00	6.3 M_b	Papua New Guinea
	27/06/2022	12	20	1.01	2.10	240	0.5	242.20	Reliable	32.945	69.474	10.00	5.9 M_l	Pak–Afghan Border
	29/06/2022	12	50	1.20	2.66	600	0.2	720.00	Reliable	36.248	70.699	223.0	5.2 M_l	Hindu Kush, Afghanistan
CE14	07/02/2021	11	50	3.63	4.20	550	0.2	1853.50	Reliable	−2.830	144.390	50.00	6.3 M_b	Papua New Guinea
	27/06/2022	12	50	3.53	3.75	240	0.5	724.80	Reliable	32.945	69.474	10.00	5.9 M_l	Pak–Afghan Border
	29/06/2022	12	50	3.83	3.68	600	0.2	2124.0	Reliable	36.248	70.699	223.0	5.2 M_l	Hindu Kush, Afghanistan

[1]No. of windows, [2]Length of window (sec), [3]H/V Peak Frequency (Hz), [4]H/V Amplitude at peak frequency, [5]No. of cycles.

Table 4.3: Processing parameters for HVSR calculation for ambient noise of Muzaffargarh area (Stations CE19 to CE23) and CE14 station.

Station	**Date**	**HH:MM:SS**	^1n_w	^2l_w	$^3f_0$	$^4A_0 > 2$	^5n_c	$f \geq 10/l_w$	$n_c \cdot (f_0) > 200$	**Remarks**
CE19	04/05/2022	10:00:00.0	59	60	0.98	2.96	3540	0.17	3469	Reliable
		22:00:00.0	59	60	1.04	2.83	3540	0.17	3682	Reliable
	05/05/2022	10:00:00.0	59	60	0.96	3.01	3540	0.17	3398	Reliable
		22:00:00.0	59	60	0.92	3.10	3540	0.17	3257	Reliable
CE20	04/05/2022	10:00:00.0	59	60	1.01	2.90	3540	0.17	3575	Reliable
		22:00:00.0	59	60	0.97	2.63	3540	0.17	3434	Reliable
	05/05/2022	10:00:00.0	59	60	1.01	3.00	3540	0.17	3575	Reliable
		22:00:00.0	59	60	0.92	2.45	3540	0.17	3257	Reliable
CE21	04/05/2022	10:00:00.0	59	60	0.90	2.44	3540	0.17	3186	Reliable
		22:00:00.0	59	60	0.91	2.45	3000	0.17	2730	Reliable
	05/05/2022	10:00:00.0	59	60	0.94	2.66	3540	0.17	3328	Reliable
		22:00:00.0	59	60	0.87	2.30	3540	0.17	3080	Reliable
CE22	04/05/2022	10:00:00.0	59	60	1.03	2.88	3540	0.17	3646	Reliable
		22:00:00.0	59	60	1.03	2.44	3540	0.17	3646	Reliable
	05/05/2022	10:00:00.0	59	60	1.01	2.90	3540	0.17	3575	Reliable
		22:00:00.0	59	60	0.94	2.44	3540	0.17	3328	Reliable
CE23	04/05/2022	10:00:00.0	59	60	1.01	3.40	3540	0.17	3575	Reliable
		22:00:00.0	59	60	1.11	3.13	3540	0.17	3929	Reliable
	05/05/2022	10:00:00.0	59	60	1.03	3.56	3540	0.17	3646	Reliable
		22:00:00.0	59	60	1.02	2.84	3540	0.17	3611	Reliable
CE14	04/05/2022	10:00:00.0	59	60	3.84	4.03	3540	0.17	12709	Reliable
		22:00:00.0	59	60	3.74	2.83	3540	0.17	12850	Reliable
	05/05/2022	10:00:00.0	59	60	3.72	4.01	3540	0.17	13027	Reliable
		22:00:00.0	59	60	3.70	2.78	3540	0.17	11611	Reliable

(1) No. of windows, (2) Length of window (sec.), (3) H/V Peak Frequency (Hz), (4) H/V Amplitude at peak frequency, (5) No. of cycles.

stations. The study area is part of Sulaiman Foredeep that consists of alluvial and eolian deposits above the deep buried basement rock. Neither borehole nor geotechnical data is available for these sites. The empirical results of soft sediment thickness in Muzaffargarh are then compared with seismic station installed on hard rock (CE14), not far away from the study region. Overall results of the analyzed data show clear and distinguishable peaks at both these locations. At Muzaffargarh area the fundamental frequency peak is observed around 1 Hz while at CE14 station, located on hard rock, a prominent peak is displayed at relatively higher frequency (> 3 Hz) compared to stations of Muzaffargarh array.

Three events (one teleseismic and two local) are analyzed to study the effect of source to receiver distance on HVSR values. The amplitude, frequency content, energy of different phases and ellipticity of waves are strongly dependent on distance. Papua New Guinea (PNG) earthquake (teleseismic) of magnitude 6.2 M_b consists of dominant surface waves that produced distinguishable peaks (Figure 5.1). For this event, Muzaffargarh seismic stations (CE19, CE20 and CE23) exhibit fundamental site frequencies in range of 1.01 Hz to 1.12 Hz with corresponding amplitudes range of 3.08 to 3.31. Whereas, CE14 station shows a clear peak with fundamental site frequency at 3.63 Hz and amplitude of 4.20. HVSR curves for Pak–Afghan border (depth $\sim$ 15 km, Figure 5.2) and Hindu Kush (depth $\sim$ 200 km, Figure 5.3) earthquakes (Afghanistan) of magnitude 5.9 M_l and 5.2 M_l respectively show less dominant amplitude compared to PNG event (Figure 5.4).

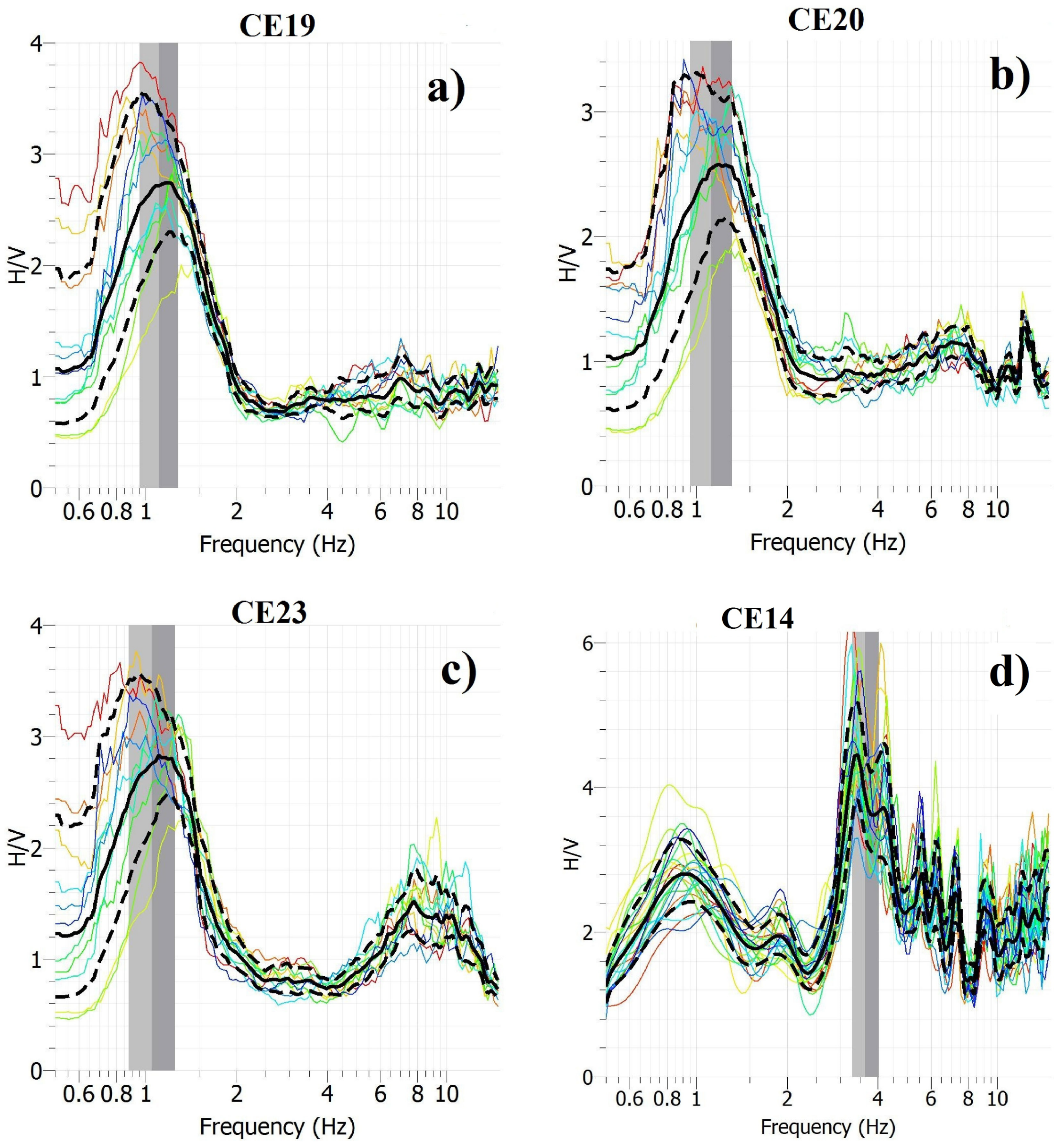

Fig. 5.1: H/V spectrum plot for Papua New Guinea earthquake of magnitude 6.3 M_b with mean (solid line) and standard deviation (dashed lines) of Muzaffargarh array (sub-figures a to c) and CE14 station (sub-figure d) installed on hard rock. Plots are statistically calculated from each time window's HVSR (colored lines). The peak frequency of average HVSR spectra and standard deviation associated with the variability of the peak frequency values from the individual curves is indicated by vertical grey shading.

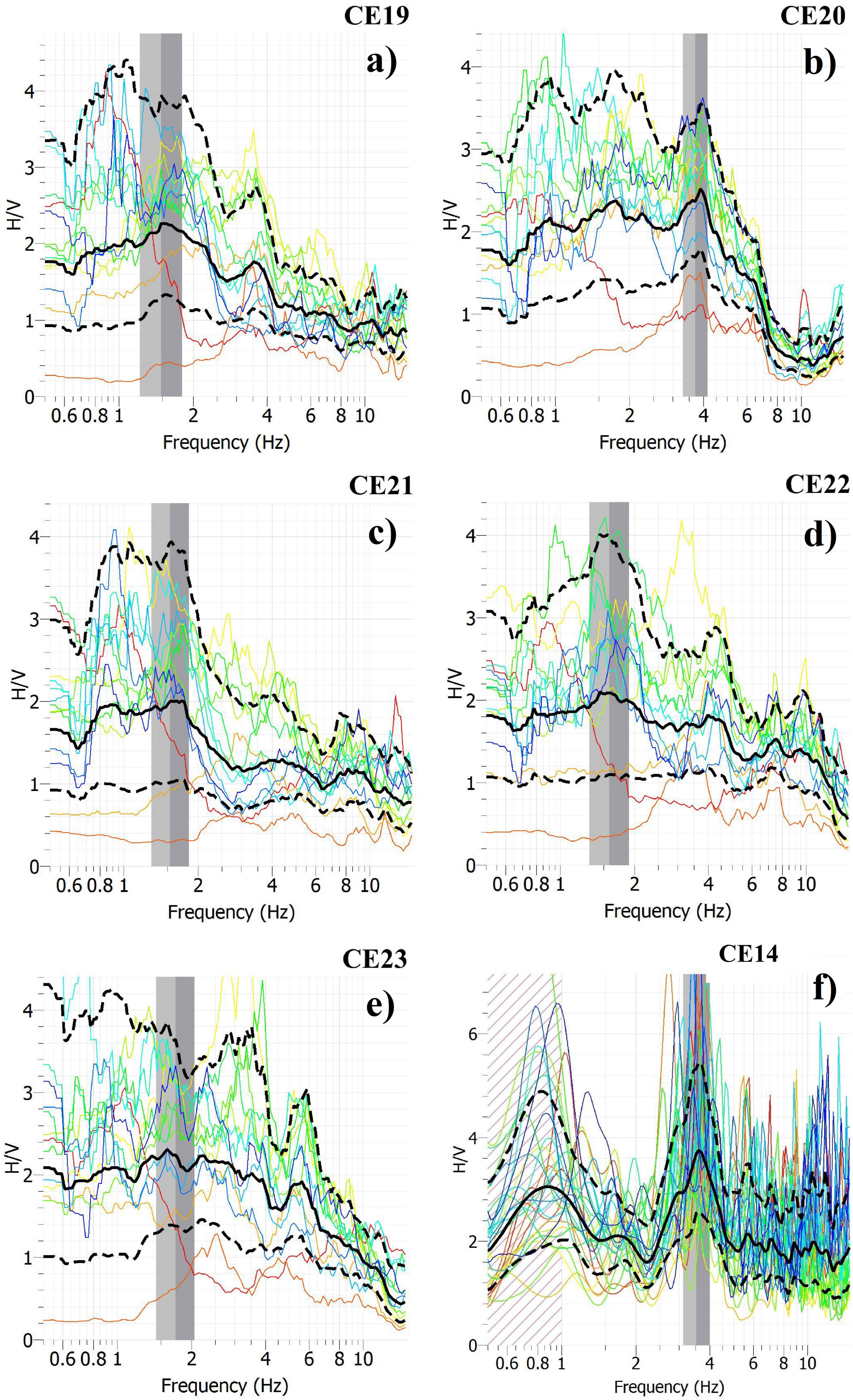

Fig. 5.2: H/V spectrum plot of Muzaffargarh Array (sub-figures a to e) and CE14 station (sub-figure f) for Pak–Afghan border, Afghanistan earthquake of Magnitude 5.9 M_l along with their fundamental site frequency and amplitude.

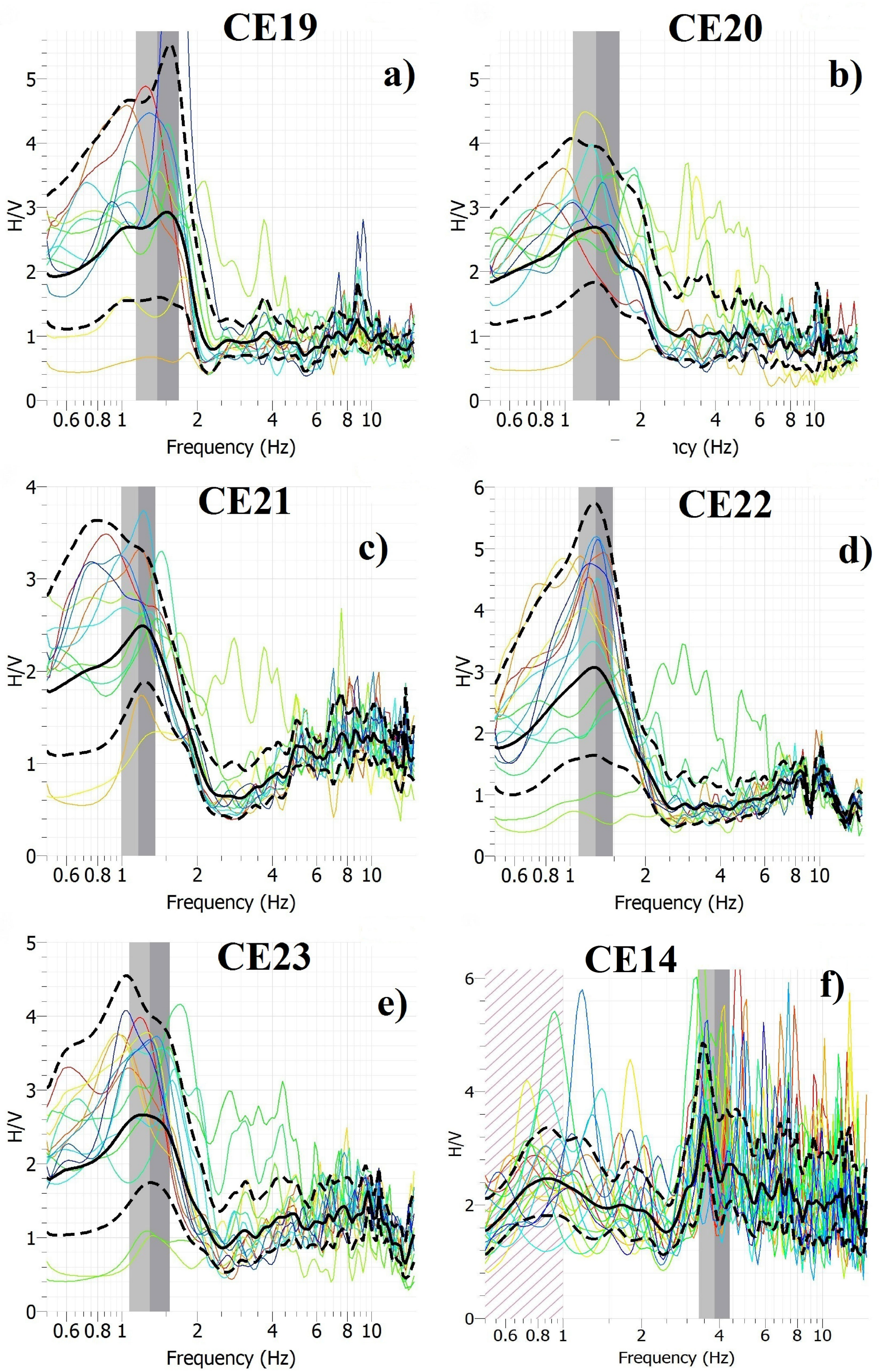

Fig. 5.3: H/V spectrum plot of Muzaffargarh Array (sub-figures a to e) and CE14 station (sub-figure f) for Hindu Kush, Afghanistan earthquake of magnitude 5.1 M_l.

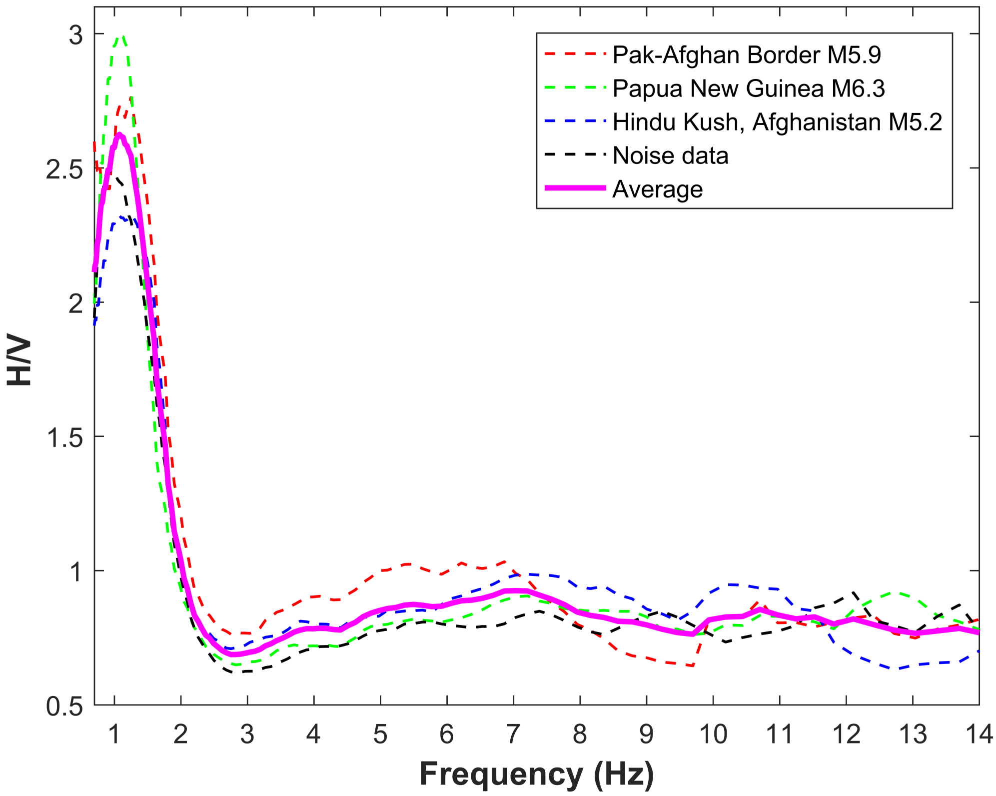

Fig. 5.4: HVSR spectrum plot for Muzaffargarh array of seismic events (discussed above) along with the average HVSR spectra. Ambient noise data HVSR spectra is also plotted. The overall trend of the plot is almost the same showing that fundamental site frequency is independent of the source (earthquake or ambient noise) being considered.

Local and shallow seismic event (Pak–Afghan border) dominantly consists of body waves but follows the similar trend of teleseismic event with peaks in frequency range of 1.01 Hz to 1.46 Hz at Muzaffargarh stations (CE19, CE20, CE21, CE22 & CE23). For Hindu Kush earthquake, the frequency and amplitude ranges are 1.17 Hz to 1.32 Hz and 2.12 to 2.94 respectively. The fundamental frequencies of Pak-Afghan border and Hindu Kush earthquakes at CE14 station are 3.53 Hz and 3.83 Hz and their corresponding amplitude values are 3.75 and 3.68 respectively (Table 4.2).

In addition to seismic events, ambient noise data of day and night time on the Muzaffargarh array are also utilized for HVSR calculation. Compared to seismic events, a much clear and distinguishable bell-shaped curves are obtained using ambient noise data (Figures 5.5 to 5.9). The fundamental site frequencies range are 0.90 Hz to 1.03 Hz and 0.87 Hz to 1.11 Hz for day and night time noise data respectively (Table 4.3).

HVSR analysis of CE14 station is also carried out to observe the difference in fundamental site frequencies between soft soil and hard rock sites. The curves for this station show clear peaks in frequency range of 3.53 Hz to 3.83 Hz and 3.70 Hz to 3.84 Hz for earthquake and ambient noise data respectively. Multiple peaks at frequencies higher than the fundamental site frequency are also noted at this location.

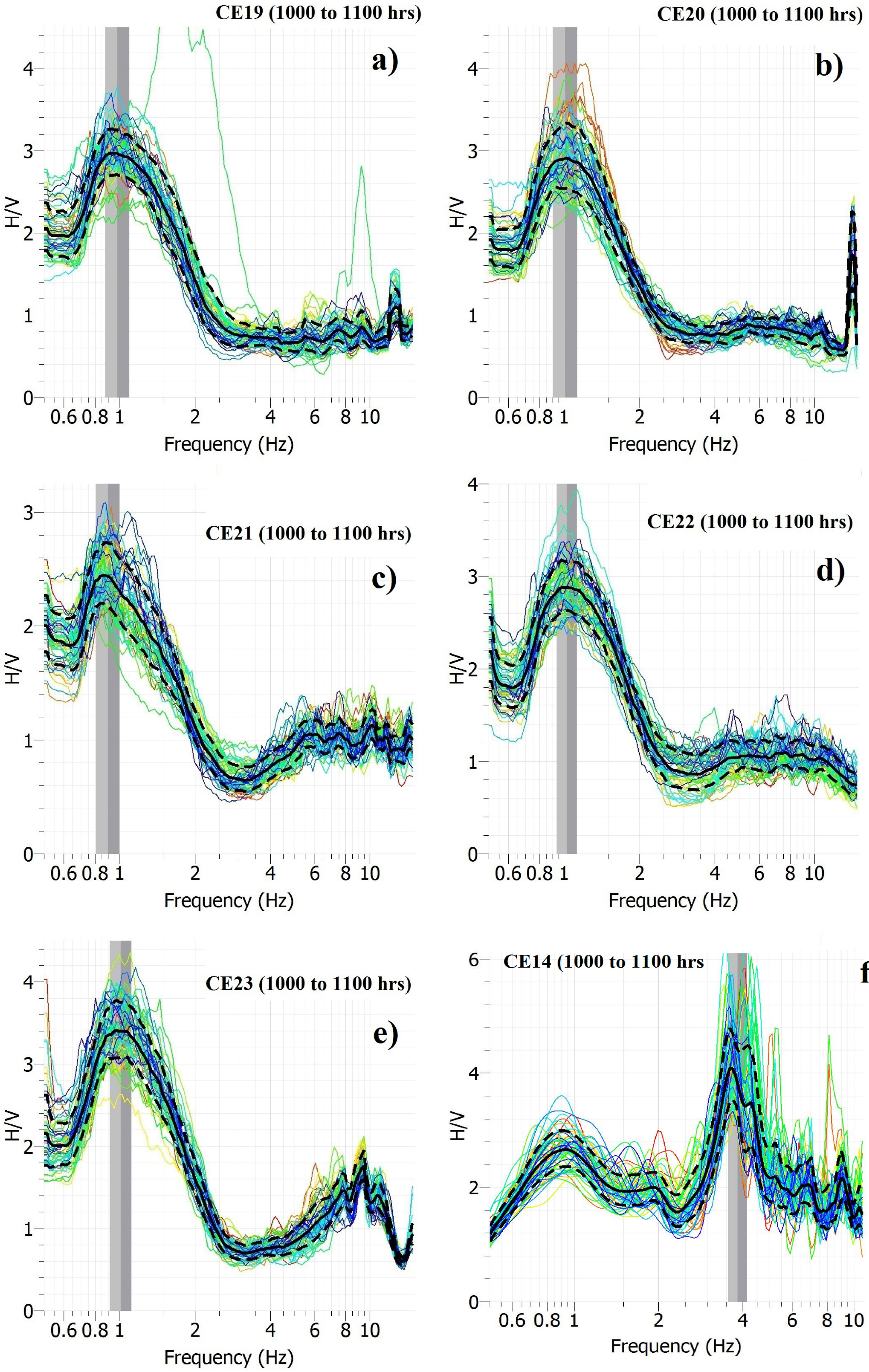

Fig. 5.5: H/V spectrum plot of Muzaffargarh Array (sub-figures a to e) and CE14 station (sub-figure f) showing fundamental frequency and their corresponding amplitude for day time ambient noise recorded on 4th May, 2022.

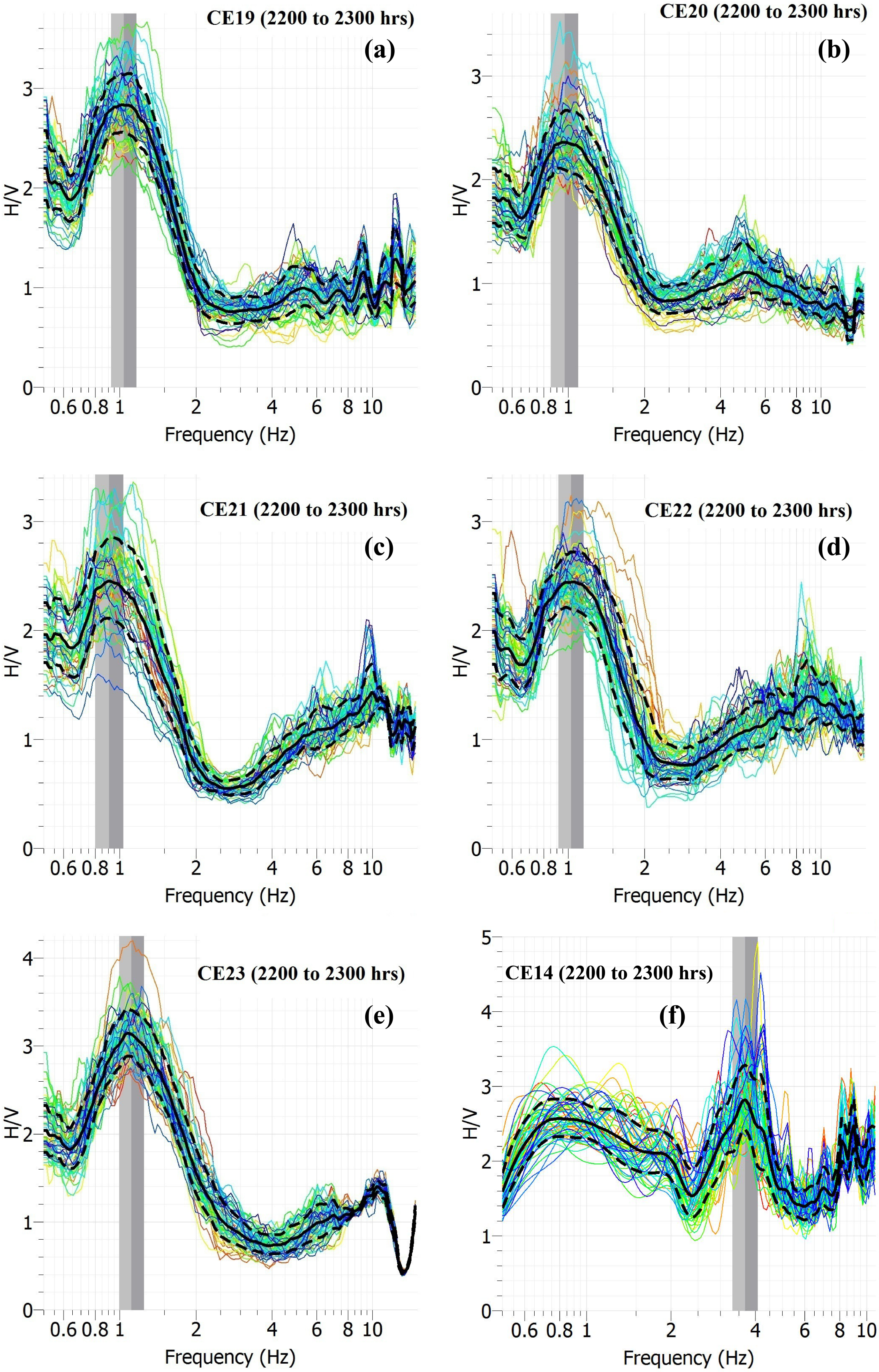

Fig. 5.6: H/V spectrum plot of Muzaffargarh Array (sub-figures a to e) and CE14 station (sub-figure f) for night time ambient noise recorded on 4th May, 2022.

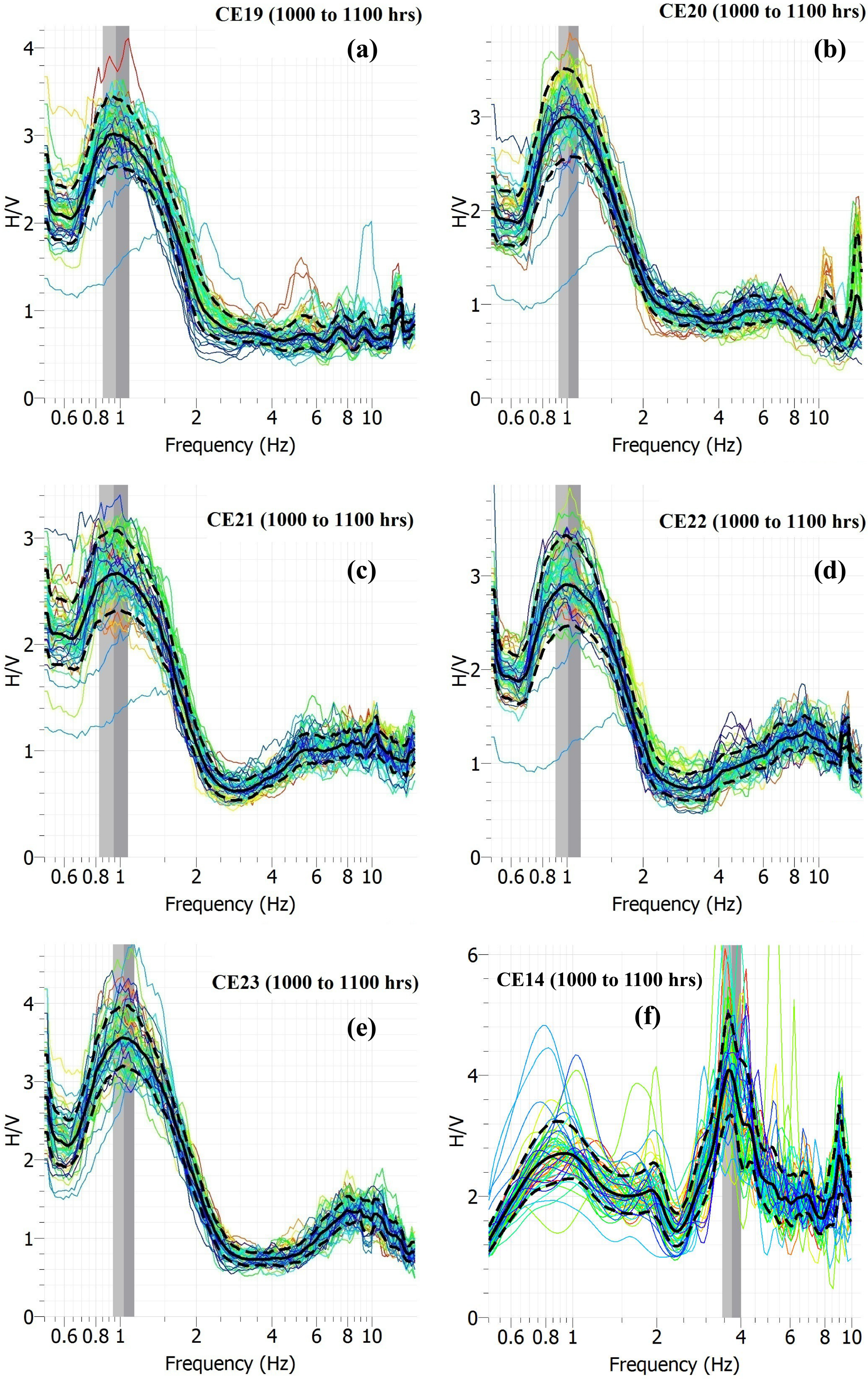

Fig. 5.7: H/V spectrum plot of Muzaffargarh Array (sub-figures a to e) and CE14 station (sub-figure f) for day time ambient noise recorded on 5th May, 2022.

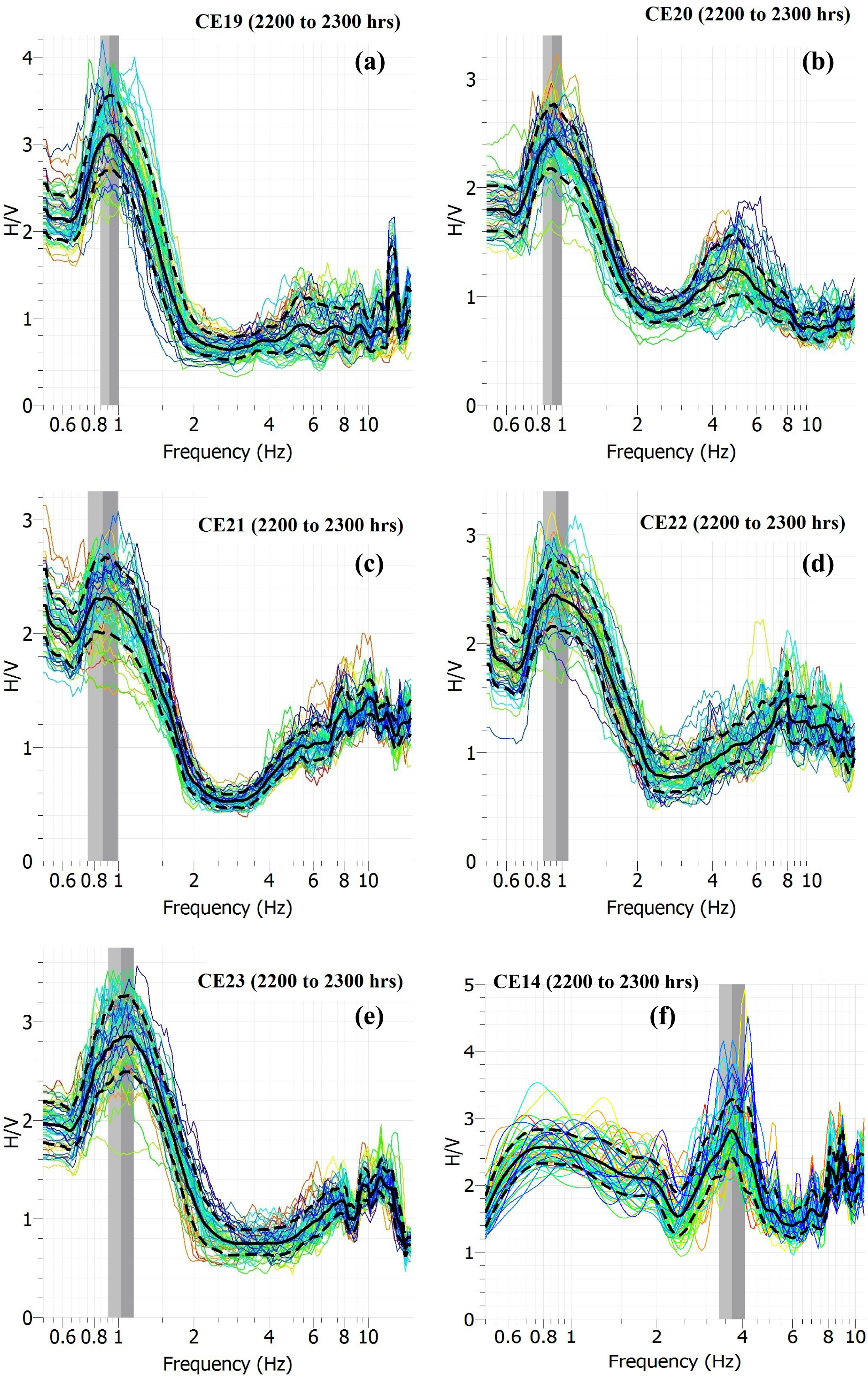

Fig. 5.8: H/V spectrum plot of Muzaffargarh Array (sub-figures a to e) and CE14 station (sub-figure f) for night time ambient noise recorded on 5th May, 2022.

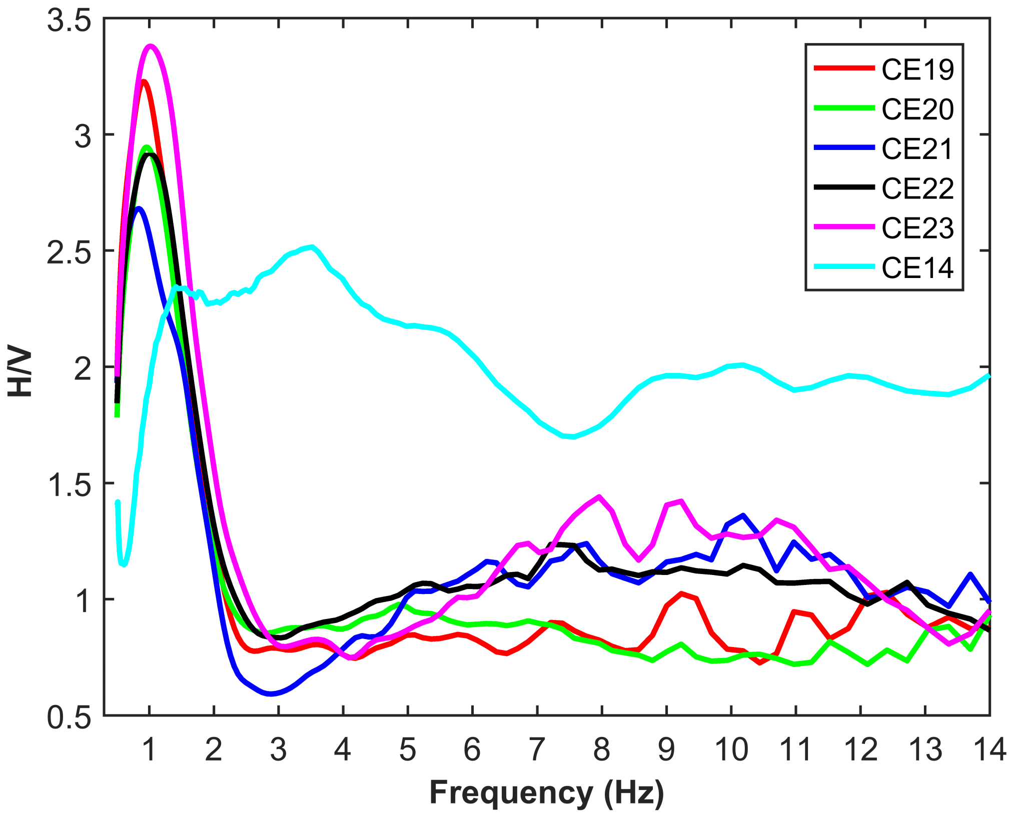

Fig. 5.9: Average HVSR noise plots of seismic stations of Muzaffargarh area and CE14 station. Note the clearly distinguishable peaks at low fundamental frequency of seismic stations installed on soft soils. CE14 station exhibit a flat curve due to low impedance contrast.

6 Discussion

Spectral ratios carried out at Muzaffargarh stations and another station at hard-rock produce H/V peak frequencies that highlight the characteristics of that area. A single and clear peak at relatively low frequency which is identified at Muzaffargarh area depict an indication of a single strong impedance contrast that exists at the interface of soil and bedrock (*Cara et al.*, 1973; *Ansary et al.*, 1995; *Volant et al.*, 1998; *Bard*, 1998; *Bignardi et al.*, 2016; S. *Khan and* M. *Khan*, 2016). This observation of a clear peak is consistent with the local geology of the area which is covered by thick layer of soil. The lateral and vertical existence of thick soil layer overlying the basement rock in this region is also responsible for attenuation of high frequencies (*Castellaro and Mulargia*, 2009; *Chen et al.*, 2009; *Hellel et al.*, 2010; *Liu et al.*, 2014; *Kwak et al.*, 2017). Stations that are installed on hard-rock their fundamental frequency is observed at higher value, due to weak impedance contrast in subsurface (*D'Amico et al.*, 2008). Normally, similar amplitudes on horizontal and vertical components observed at hard site depict no amplification. The fundamental site frequency of CE14 station is clearly higher than whole of the Muzaffargarh area (Table 4.2). This disparity in frequencies can be easily interpreted as difference between the hard rock covered by a thin layer of soil (CE14 station) and a dense layer of sediments covering the area of Muzaffargarh (*Hellel et al.*, 2010). In addition to high fundamental site frequency, we also observe more than one peaks in the HVSR spectra of CE14 station. These peaks appear in all the HVSR calculations made for this site. The multiple peaks observed in our case could have been originated by any of the reasons like, multiplicity of local maxima (*Guégüen et al.*, 1998; *Bodin et al.*, 2001; *Lebrun et al.*, 2001; *Woolery and Street*, 2002; *Asten*, 2004; *Oliveto et al.*, 2004), presence of complex subsurface structures (*Castellaro and Mulargia*, 2009), acoustic impedance contrasts at different depths and lateral subsurface variations (*Kang et al.*, 2020a), or even Rayleigh waves (*Nakamura*, 1989).

A slight and barely noticeable amplitude variation of noise data during day and night time (2.96 and 2.83 for day and night times noise respectively) is observed at CE19 station. Similar, pattern of amplitude fluctuations at the remaining Muzaffargarh seismic stations also prevailed, showing invariant nature of site conditions (Table 4.3). The elevated cultural noise and anthropogenic activities are more pronounced during the day time that might cause increase in amplitude. Furthermore, various sources of noises may also contribute to variations observed in the amplitude. This is due to the reason that waves arriving at any seismic station have variable sources and thus have varying degree of share in composition of the ambient noise. These different percentages of waves in ambient noise is another explanation for variations in amplitude recorded by the same station. However, regardless of the time of day, the ambient noise yielded similar results of HVSR, i.e., the fundamental site frequency, more or less, remains the same despite changes in frequency characteristics over the course of day and night.

A comparison of average HVSR spectra based on ambient noise data (day and night) of different seismic stations used in this study is shown in Figure 5.9. Stations installed on soft sediments produce a clear peak at low frequency (~ 1 Hz) compared to CE14 station which exhibited peak at relatively higher frequency ($> 3\,\mathrm{Hz}$). Although, amplitudes of Muzaffargarh region stations are different from each other but have rather similar fundamental site frequency. The CE23 has higher amplitude and broad peak of HVSR curve compared to CE21 station that has relatively lower amplitude and narrow peak. Different nature of noise source and lateral variation of substrata among these stations may result in such variations. Furthermore, at high frequency values CE20 and CE22 stations produce flat lines while CE19, CE 21 and CE23 show a series of smaller peaks. Moreover, the fundamental site frequencies of either rock or soft soil stations are independent of source to receiver distance (Figure 6.1).

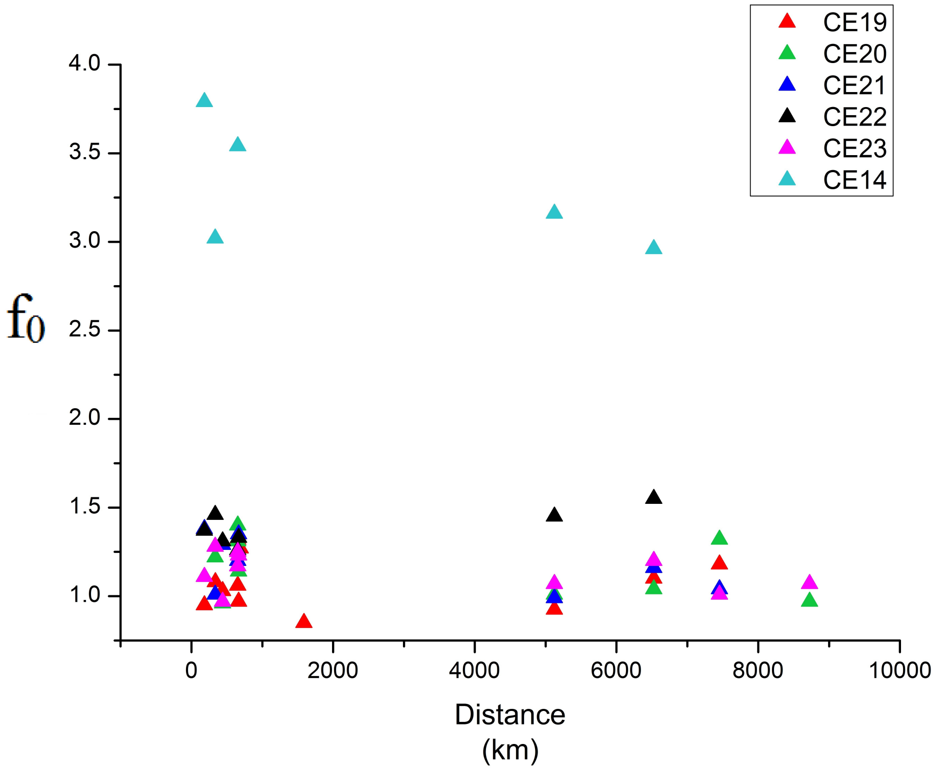

Fig. 6.1: Fundamental site frequencies of Muzaffargarh array and CE14 plotted against distance. All events ranging from telesesimic to local are considered for examining the fundamental frequency dependency on distance.

The simplest relation existing in earthquake engineering for calculating a structure's natural time period is $N = 10 \times T_0$ (*Housner and Brady*, 1963) where N is the number of floors while T_0 represents the natural time period of the building. In this area, the natural period of 9 to 10 floor buildings have a high chance of coinciding with the natural time period of subsurface strata. This will result in increased oscillation of the building and consequently a greater chance of experiencing damage or even collapsing. Construction of such buildings should be avoided in this region due to their high vulnerability to ground motion (*Michel et al.*, 2010).

6.1 Seismic Vulnerability Index

The intensity, frequency and duration of ground motions are some factors that determine the amount of damages during an earthquake. Therefore, it is vital to identify buildings or areas that are prone to earthquake shaking. The 'seismic vulnerability index (K_g)' is an important parameter that represents the vulnerability value of ground surface and buildings during earthquake (*Abd El-Aal*, 2010; *Liu et al.*, 2014). The K_g was highest (9.63) and lowest (3.61) at CE23 and CE14 stations respectively (Table 6.1). Reclaimed or soft sediment region has higher K_g values as compared to hard rock region. Such regions are seismically vulnerable and have high chances of experiencing damages during an earthquake due to amplification of incident waves. However, it may be noted that the HVSR peak amplitude overestimates/underestimates the amplification factor of the site and it must not be considered an absolute amplification value (*Rong et al.*, 2017; *Kang et al.*, 2020b). During 1989 M_w 6.9 Loma Prieta earthquake, several damages to buildings was observed at the Marina District of San Francisco (USA), characterized by higher K_g value ($K_g > 20$). Majority of subsurface sediments of the Marina District were landfill, made up of fine and silty sands (R. *Seed et al.*, 1991). While, areas having lower K_g value ($K_g < 20$) minimal damage was observed (*Nakamura*, 1997; *Liu et al.*, 2014). Similarly, during 1999 M_w 7.7 Chi-Chi earthquake (Taiwan), higher K_g value ($K_g > 10$) regions exhibit large scale liquefactions and several damages during an earthquake (*Huang and Tseng*, 2002). The K_g value is a relative term and can't be interpreted directly in terms of damages.

Table 6.1: Seismic vulnerability index (K_g) calculated for soil (stations CE19 to CE23) and hard-rock (station CE14) by using the amplitude A_0 and fundamental site frequency f_0.

Station Name	A_0	f_0 (Hz)	K_g
CE19	2.88	0.97	8.55
CE20	2.68	0.98	7.33
CE21	2.50	0.93	6.72
CE22	2.70	1.00	7.29
CE23	3.15	1.03	9.63
CE14	3.67	3.73	3.61

6.2 Soil thickness from HVSR

Ahmed and Ghazi (2022) has classified this region as class D (stiff soil) by following the codes of Building Codes of Pakistan, 2007 and having V_{S30} values in the range of $175\,\mathrm{m\,s^{-1}}$ to $350\,\mathrm{m\,s^{-1}}$.

Similarly, *Zaman and Warnitchai* (2016) reported, near-surface shear wave velocity of the area in range of $180\,\mathrm{m\,s^{-1}}$ to $240\,\mathrm{m\,s^{-1}}$. This value of V_{S30} is used to get the thickness of soil layer in this area using the following relation:

$$f_0 = \frac{V_{S30}}{4h} \tag{6.1}$$

Here, f_0 is fundamental site frequency in Hz, V_{S30} is shear wave velocity in m/s and h is depth to soil-bedrock interface in meters (*Lachet and Bard*, 1994; *Ibs-von Seht and Wohlenberg*, 1999; *Lee et al.*, 2017). Soil thickness using average values of fo of each station of Muzaffargarh array is computed in Table 6.2. Approximately, 60 m of soil cover is estimated using both of the above mentioned V_{S30} values. Although, there is room for improvement in the interpretation of bedrock depth through development of regression equations that are coherent with local settings of the study area.

Table 6.2: Soil thickness (h) calculated for Muzaffargarh Array using the average fundamental site frequency value for each station (h_1 values are calculated by taking minimum and maximum V_{S30} values of 175 m s^{-1} to 350 m s^{-1} from *Ahmed and Ghazi* (2022), h_2 values are calculated using minimum and maximum V_{S30} of 180 m s^{-1} to 240 m s^{-1} from *Zaman and Warnitchai* (2016), and h_{avg} is the average value of h_1 and h_2).

Station	f_0 (Hz)	h_1 (m)	h_2 (m)	h_{avg} (m)
CE19	1.10	40.00–79.50	49.50–66.00	59
CE20	1.15	38.00–76.00	51.75–69.00	59
CE21	1.18	37.00–74.00	53.10–70.80	59
CE22	1.15	38.00–76.00	51.75–69.00	59
CE23	1.39	31.50–63.00	62.55–83.40	60

7 *Conclusions*

The seismic microzonation of the Muzaffargarh region is performed using five seismic stations at soft sediments and one station at hard rock used for comparison. The obtained fundamental site frequency and amplitude observed on different stations are interpreted for seismic vulnerability index. The HVSR curves for Muzaffargarh array obtained by using earthquake and ambient noise data are mostly similar. Lower values of fundamental frequency of Muzaffargarh region (1.01 Hz to 1.46 Hz and 0.87 Hz to 1.11 Hz for earthquakes and ambient noise respectively), indicate the presence of unconsolidated and homogeneous sedimentary cover in the region. The presence of soil layer could greatly amplify ground motion in case of an earthquake and consequently greater the seismic risk. Sedimentary cover in Muzaffargarh area estimated from average value of fundamental frequencies of these stations is about 60 m. The fundamental site frequency of an area is independent of distance of the seismic event, whether it is teleseismic or local. K_g values are higher in areas of thick sedimentary cover and therefore, represent seismically vulnerable zones. Low values are observed in areas of thin sedimentary cover or hard rock. The lower the K_g value, lower will be the influence of site effect and hence lower will be the risk of damage during an earthquake. However, these results should be calibrated by comparisons with borehole data by employing detailed information of local subsurface geology. This will help in providing reliable sediment depth estimates of the region which is useful for calculation of seismic response of civil structures, seismic hazard assessment and earthquake mitigation.

Acknowledgements, Samples, and Data

The authors are grateful to the Director General (CES) for provision of data used in this study. The authors are also thankful to Zafar Iqbal, Naveed Mushtaq and Muhammad Yousaf Khan for their assistance in improving this manuscript technical writing.

Seismograms used in this study are taken from Centre for Earthquake Studies (CES) and local seismic network of Pakistan Metrological Department (PMD).

Funding

This research did not receive any specific grant from funding agencies in the public, commercial, or not-for-profit sectors.

References

Abd El-Aal, A., 2010. Modelling of Seismic Hazard at the North-Eastern Part of Greater Cairo Metropolitan Area, Egypt. *Journal of Geophysics and Engineering*, **7**, 75–90.

Adib, A., P. Afzal and K. Heydarzadeh, 2015. Site Effect Classification Based on Microtremor Data Analysis Using a Concentration–Area Fractal Model. *Nonlinear Process Geophysics*, **22** (1), 53–63.

Ahmed, N. and S. Ghazi, 2022. Comparison of DSHA-based Response Spectrum with Design Response Spectrum of Building Code of Pakistan (BCP-SP-2007) for a Site in Muzaffargarh Area, Pakistan. *Earthquake Science*, 280–292.

Aitchison, J., J. Ali and A. Davis, 2007. When and Where Did India and Asia Collide? *Journal of Geophysical Research: Solid Earth*, **112** (B5).

Aki, K. and P. Richards, 2002. *Quantitative Seismology: Theory and Methods*. University Science Books.

Alfaro, A., L. G. Pujades, X. Goula, T. Susagna, M. Navarro, J. Sánchez and J. A. Canas, 2002. “Preliminary Map of Soil’s Predominant Periods in Barcelona Using Microtremors”. In: *Earthquake Microzoning*. Ed. by A. Roca and C. Oliveira. Basel: Birkhäuser Basel, 2499–2511. ISBN: 978-3-0348-8177-7.

Ansary, M., F. Yamazaki, M. Fuse and T. Katayama, 1995. *Use of Microtremors for the Estimation of Ground Vibration Characteristics*. St. Louis, Missouri. 2.

Asten, M., 2004. Comment on ‘Microtremor Observations of Deep Sediment Resonance in Metropolitan Memphis, Tennessee’ by Paul Bodin, Kevin Smith, Steve Horton and Howard Hwang. *Engineering Geology*, **72**, 343–349.

Bard, P.-Y., Dec. 1998. “Microtremor measurements: A tool for site effect estimation?” In: *The effects of surface geology on seismic motion*. Vol. 3, 1251–1279.

Bender, F. and H. Raza, 1995. *Geology of Pakistan*.

Bernard, M., B. Shen-Tu, W. Holt and D. Davis, 2000. Kinematics of Active Deformation in the Sulaiman Lobe and Range, Pakistan. *Journal of Geophysical Research: Solid Earth*, **105** (B6), 13253–13279.

Beroya, M., A. Aydin, R. Tiglao and M. Lasal, 2009. Use of Microtremor in Liquefaction Hazard Mapping. *Engineering Geology*, **107** (3), 140–153.

Bignardi, S., A. Mantovani and N. Zeid, 2016. OpenHVSR: Imaging the Subsurface 2D/3D Elastic Properties Through Multiple HVSR Modeling and Inversion. *Computers & Geosciences*, **93**, 103–113.

Bindi, D. *et al.*, 2011. The Influence of Site Amplification on Ground Motion Prediction in the Context of the European Seismic Hazard Model. *Geophysical Journal International*, **186** (3), 1335–1346.

Bodin, P., K. Smith, S. Horton and H. Hwang, 2001. Microtremor Observations of Deep Sediment Resonance in Metropolitan Memphis, Tennessee. *Engineering Geology*, **2**, 159–168.

Bonilla, L., J. Steidl, G. Lindley, A. Tumarkin and R. Archuleta, 1997. Site Amplification in the San Fernando Valley, California: Variability of Site-Effect Estimation Using the S-wave, Coda, and H/V Methods. *Bulletin of the Seismological Society of America*, **87** (3), 710–730.

Bonnefoy-Claudet, S., C. Cornou, P.-Y. Bard, F. Cotton, P. Moczo, J. Kristek and D. Fah, 2006. H/V ratio: a tool for site effects evaluation. Results from 1-D noise simulations. *Geophysical Journal International*, **167**, 827–837. DOI: 10.1111/j.1365-246X.2006.03154.x.

Boore, D., 2003. Simulation of Ground Motion in the Near-Source Region. *Pure and Applied Geophysics*, **160** (3), 463–480.

Bouchon, M., 1981. Seismic waves trapped in the sedimentary layers of the Earth. *Journal of Geophysical Research*, **86** (B7), 6195–6202.

Bour, M., D. Fouissac, P. Dominique and C. Martin, 1998. On the use of microtremor recordings in seismic microzonation. *Soil Dynamics and Earthquake Engineering*, **17** (7-8), 465–474.

Cakir, R. and T. Walsh, 2012. Shallow seismic site characterizations at 25 ANSS/PNSN stations and compilation of site-specific data for the entire strong motion network in Washington and Oregon. Tech. rep.

Cara, F., G. Di Giulio and A. Rovelli, 1973. A study on seismic noise variations at Colfiorito, central Italy: implications for the use of H/V spectral ratios. *Geophysical Research Letters*, **30** (18).

Castellaro, S. and F. Mulargia, 2009. VS30 estimates using constrained H/V measurements. *Bulletin of the Seismological Society of America*, **99** (2A), 761–773.

Chatelain, J. and B. Guillier, 2013. Reliable fundamental frequencies of soils and buildings down to 0.1 Hz obtained from ambient vibration recordings with a 4.5-Hz sensor. *Seismological Research Letters*, **84** (2), 199–209.

Chen, Q., L. Liu, W. Wang and E. Rohrbach, 2009. Site effects on earthquake ground motion based on microtremor measurements for metropolitan Beijing. *Chinese Science Bulletin*, **54** (2), 280–287.

Copley, A., J. Avouac and J. Royer, 2010. India-Asia collision and the Cenozoic slowdown of the Indian plate: Implications for the forces driving plate motions. *Journal of Geophysical Research: Solid Earth*, **115** (B3).

D'Amico, V., M. Picozzi, F. Baliva and D. Albarello, 2008. Ambient noise measurements for preliminary site-effects characterization in the urban area of Florence, Italy. *Bulletin of the Seismological Society of America*, **98** (3), 1373–1388.

DeMets, C., R. Gordon, D. Argus and S. Stein, 1990. Current plate motions. *Geophysical Journal International*, **101** (2), 425–478.

Edwards, C., 2006. Thailand lifelines after the December 2004 Great Sumatra earthquake and Indian Ocean tsunami. *Earthquake Spectra*, **22**, 641–659.

Fäh, D., M. Wathelet, M. Kristekova, H. Havenith, B. Endrun, G. Stamm, V. Poggi, J. Burjánek and C. Cornou, 2009. Using ellipticity information for site characterisation. *NERIES JRA4 "Geotechnical Site Characterisation"*. Task B 2.

Fat-Helbary, R.-S., K. El-Faragawy and A. Hamed, 2019. Application of HVSR technique in the site effects estimation at the south of Marsa Alam city, Egypt. *Journal of African Earth Sciences*, **154**, 89–100.

Field, E. and K. Jacob, 1993. The theoretical response of sedimentary layers to ambient seismic noise. *Geophysical Research Letters*, **20** (24), 2925–2928.

Frankel, A., 1993. Three-dimensional simulation of ground shaking in the Los Angeles Basin. *Journal of Geophysical Research*, **98** (B4), 6671–6697.

Garofalo, F., S. Foti, F. Hollender, P. Bard, C. Cornou, B. Cox, M. Ohrnberger, D. Sicilia, M. Asten and G. Giulio, 2016. InterPACIFIC project: Comparison of invasive and non-invasive methods for seismic site characterization. Part I: Intra-comparison of surface wave methods. *Soil Dynamics and Earthquake Engineering*, **82**, 222–240.

Goda, K., T. Rossetto, N. Mori and S. Tesfamariam, 2018. *Mega quakes: Cascading earthquake hazards and compounding risks*. Frontiers Media SA, 8.

Gomberg, J. *et al.*, 2005. Microzonation of Seismic Hazard in the San Francisco Bay Area: Site Response from Shallow Velocity Profiles. *Journal of Seismology*, **9** (4), 521–532.

Gripp, A. and R. Gordon, 1990. Current plate velocities relative to the hotspots incorporating the NUVEL-1 global plate motion model. *Geophysical Research Letters*, **17** (8), 1109–1112.

Guéguen, P., J.-L. Chatelain, B. Guillier and H. Yepes, 2000. An indication of the soil topmost layer response in Quito (Ecuador) using noise H/V spectral ratio. *Soil Dynamics and Earthquake Engineering*, **19** (2), 127–133.

Guégüen, P., J.-L. Chatelain, B. Guillier, H. Yepes and J. Egred, 1998. Site effect and damage distribution in Pujili (Ecuador) after the 28 March 1996 earthquake. *Soil Dynamics and Earthquake Engineering*, **17**, 329–334.

Guillier, B., J.-L. Chatelain, H. Tavera, H. Perfettini, A. Ochoa and B. Herrera, 2014. Establishing empirical period formula for RC buildings in Lima, Peru: Evidence for the impact of both the 1974 Lima earthquake and the application of the Peruvian seismic code on high-rise buildings. *Seismological Research Letters*, **85** (6), 1308–1315.

Gupta, R., M. Agrawal, S. Pal and M. Das, 2021. Seismic site characterization and site response study of Nirsa (India). *Natural Hazards*, **108** (2), 2033–2057.

Gupta, R., M. Agrawal, S. Pal, R. Kumar and S. Srivastava, 2019. Site characterization through combined analysis of seismic and electrical resistivity data at a site of Dhanbad, Jharkhand, India. *Environmental Earth Sciences*, **78**, 1–13.

Gupta, R., M. Agrawal, S. Pal, S. Srivastava and R. Kumar, 2018. "Seismic site characterization through joint analysis of MASW and microtremor data in Dhanbad, Jharkhand, India". In: *AGU Fall Meeting Abstracts*, S23C–0544.

Haghshenas, E., P.-Y. Bard and N. Theodulidis, 2008. Empirical evaluation of microtremor H/V spectral ratio. *Bulletin of Earthquake Engineering*, **6** (1), 75–108.

Haryono, A., Sungkono, M. Caesardi, B. Santosa, F. Syaifuddin and A. Widodo, 2020. Estimation of Shear Wave Velocity Using Horizontal to Vertical Spectrum Ratio (HVSR) Inversion to Identify Faults in Pacitan. *IOP Conference Series: Earth and Environmental Science*, **506** (1).

Havskov, J., P. Voss and L. Ottemoller, 2020. 30 Yr of SEISAN. *Seismological Research Letters*, **91** (3), 1846–1852.

Hellel, M., J.-L. Chatelain, B. Guillier, D. Machane, R. Salem, E. Oubaiche and H. Haddoum, 2010. Heavier Damages without Site Effects and Site Effects with Lighter Damages: Boumerdes City (Algeria) after the May 2003 Earthquake. *Seismological Research Letters*, **81** (1).

Housner, G. and A. Brady, 1963. Natural periods of vibration of buildings. *Journal of Engineering Mechanics*, **89** (8), 31–65.

Huang, H.-C. and Y.-S. Tseng, 2002. Characteristics of soil liquefaction using H/V of microtremors in Yuan-Lin area. *Terrestrial, Atmospheric and Oceanic Sciences*, **13**, 325–338.

Humayon, M., 1990. "Structural Interpretation of the Eastern Sulaiman Foldbelt and Foredeep". MA thesis. Oregon State University.

Ibs-von Seht, M. and J. Wohlenberg, 1999. Microtremor measurements used to map thickness of soft sediments. *Bulletin of the Seismological Society of America*, **89**, 250–259.

Kanamori, H., 1977. The Energy Release in Great Earthquakes. *Journal of Geophysical Research*, **82** (20), 2981–2987.

Kang, S., K.-H. Kim, J.-M. Chiu and L. Liu, 2020a. Microtremor HVSR analysis of heterogeneous shallow sedimentary structures at Pohang, South Korea. *Journal of Geophysics and Engineering*, 861–869.

Kang, S., K.-H. Kim and B. Kim, 2020b. Assessment of seismic vulnerability using the horizontal-to-vertical spectral ratio (HVSR) method in Haenam, Korea. *Geosciences Journal*.

Kawase, H., F. Sanchez-Sesma and S. Matsushima, 2011. The optimal use of horizontal-to-vertical spectral ratios of earthquake motions for velocity inversions based on diffuse-field theory for plane waves. *Bulletin of the Seismological Society of America*.

Kazmi, A. and M. Jan, 1997. *Geology and Tectonics of Pakistan*.

Khalid, P., M. Naeem, M. Haroon Afzal, Z. Din and Q. Yasin, 2014. Petroleum Play Analysis, Structural and Stratigraphic Interpretation of Cretaceous Sequence, Punjab Platform, Central Indus Basin, Pakistan. *Science International*, **26** (5).

Khan, M., R. Bendick, M. Bhat, R. Bilham, D. Kakar, S. Khan, S. Lodi, M. Qazi, B. Singh and W. Szeliga, 2008. Preliminary geodetic constraints on plate boundary deformation on the western edge of the Indian plate from TriGGnet (Tri-University GPS Geodesy Network). *Journal of Himalayan Earth Sciences*, **41**, 71–87.

Khan, S. and M. Khan, 2016. Mapping sediment thickness of Islamabad city using empirical relationships: Implications for seismic hazard assessment. *Journal of Earth System Science*, **125** (3), 623–644.

Kwak, D., J. Stewart, S. Mandokhail and D. Park, 2017. Supplementing VS30 with H/V spectral ratios for predicting site effects. *Bulletin of the Seismological Society of America*, **107** (5), 2028–2042.

Lachet, C. and P.-Y. Bard, 1994. Numerical and theoretical investigations on the possibilities and limitations of Nakamura's Technique. *Journal of Physics of the Earth*, **42**, 377–397.

Lebrun, B., D. Hatzfeld and P.-Y. Bard, 2001. Site effect study in urban area: experimental results in Grenoble (France). *Pure and Applied Geophysics*, **158**, 2543–2557.

Lee, H., R. Kim and T.-S. Kang, 2017. Seismic response from microtremor of Chogye Basin, Korea. *Geophysics and Geophysical Exploration*, **20**, 88–95.

Lermo, J. and F. Chávez-García, 1994. Are microtremors useful in site response evaluation? *Bulletin of the Seismological Society of America*, **84** (5), 1350–1364.

Liu, L., Q.-f. Chen, W. Wang and E. Rohrbach, 2014. Ambient noise as the new source for urban engineering seismology and earthquake engineering: a case study from Beijing metropolitan area. *Earthquake Science*, **27** (1), 89–100.

Lunedei, E. and P. Malischewsky, 2015. "A review and some new issues on the theory of the H/V technique for ambient vibrations". In: *Perspectives on European Earthquake Engineering and Seismology, Geotechnical, Geological and Earthquake Engineering*.

Michel, C., P. Guéguen, P. Lestuzzi and P.-Y. Bard, 2010. Comparison between seismic vulnerability models and experimental dynamic properties of existing buildings in France. *Bulletin of Earthquake Engineering*, **8**, 1295–1307.

Molnar, S. and J. Cassidy, 2006. A comparison of site response techniques using weak-motion earthquakes and microtremors. *Earthquake Spectra*, **22** (1), 169–188.

Molnar, S., A. Sirohey, J. Assaf, P.-Y. Bard, S. Castellaro, C. Cornou, B. Cox, B. Guillier, B. Hassani, H. Kawase, S. Matsushima, F. Sanchez-Sesma and A. Yong, 2021. A review of the microtremor horizontal-to-vertical spectral ratio (MHVSR) method. *Journal of Seismology*.

Mukhopadhyay, S. and P. Bormann, 2004. Low cost seismic microzonation using microtremor data: an example from Delhi, India. *Journal of Asian Earth Sciences*, **24** (3), 271–280.

Nakamura, Y., 1989. A method for dynamic characteristics estimation of subsurface using microtremor on the ground surface. *Quarterly Report of RTRI*, **30** (1), 25–30.

Nakamura, Y., Nov. 1997. “Seismic Vulnerability Indices for Ground and Structures Using Microtremor”. In: *Proceedings of the World Congress on Railway Research*. World Congress on Railway Research (Florence, Italy).

Navarro, M., T. Enomoto, F. J. Sánchez, I. Matsuda, T. Iwatate, A. M. Posadas, F. LuzóN, F. Vidal and K. Seo, 2002. “Surface Soil Effects Study Using Short-period Microtremor Observations in Almería City, Southern Spain”. In: *Earthquake Microzoning*. Ed. by A. Roca and C. Oliveira. Basel: Birkhäuser Basel, 2481–2497. ISBN: 978-3-0348-8177-7.

O’Brien, P., N. Zotov, R. Law, M. Khan and M. Jan, 2001. Coesite in Himalayan eclogite and implications for models of India-Asia collision. *Geology*, **29** (5), 435–438.

Oliveto, A., M. Mucciarelli and R. Caputo, 2004. HVSR prospecting in multilayered environments: an example from the Tyrnavos Basin (Greece). *Journal of Seismology*, **8**, 395–406.

Pakistan, G. S. of, 1964. *Geological Map of Pakistan*.

Panzera, F., S. D’Amico, A. Lotteri, P. Galea and G. Lombardo, 2012. Seismic site response of unstable steep slope using noise measurements: the case study of Xemxija Bay area, Malta. *Natural Hazards and Earth System Sciences*, **12** (11), 3421–3431.

Panzera, F., G. Lombardo, S. D’Amico and P. Galea, 2013. Speedy Techniques to Evaluate Seismic Site Effects in Particular Geomorphologic Conditions: Faults, Cavities, Landslides and Topographic Irregularities.

Raza, H., R. Ahmed, S. Ali and J. Ahmad, 1989. Petroleum prospects: Sulaiman sub-basin, Pakistan. *Pakistan Journal of Hydrocarbon Research*, **1** (2), 21–56.

Raza, H., S. Ali and R. Ahmed, 1990. Petroleum geology of Kirthar sub-basin and part of Kutch Basin. *Pakistan Journal of Hydrocarbon Research*, **2** (1), 27–73.

Reynolds, K., A. Copley and E. Hussain, 2015. Evolution and dynamics of a fold-thrust belt: the Sulaiman Range of Pakistan. *Geophysical Journal International*, **201** (2), 683–710.

Rong, M., L. Fu, Z. Wang, X. Li, N. Carpenter and E. Wang, 2017. On the amplitude discrepancy of HVSR and site amplification from strong-motion observations. *Bulletin of the Seismological Society of America*.

Seed, H. and I. Idriss, 1970. Soil Moduli and Damping Factors for Dynamic Response Analysis. *Journal of Soil Mechanics and Foundations*, **96** (SM4), 1139–1158.

Seed, R., M. Riemer and S. Dickenson, 1991. “Liquefaction of soils in the 1989 Loma Prieta Earthquake”. In: *International Conferences on Recent Advances in Geotechnical Earthquake Engineering and Soil Dynamics*. St. Louis, 1575–1586.

Stein, S., G. Sella and E. Okal, 2002. “Plate Boundary Zones”. In: *Geodynamics Series*. Washington, DC: American Geophysical Union, 243–254.

Stokoe, K. *et al.*, 2001. Site Characterization for Liquefaction Potential Using Seismic Cone Penetrometer Testing. *Geotechnical Testing Journal*, **24** (1), 33–51.

Sugianto, N., M. Farid and W. Suryanto, 2016. Local geology condition of Bengkulu city based on seismic vulnerability index (Kg). *Journal of Engineering and Applied Sciences*, **11** (7), 4797–4803.

Theilen-Willige, B., 2010. Detection of local site conditions influencing earthquake shaking and secondary effects in Southwest-Haiti using remote sensing and GIS-methods. *Natural Hazards and Earth System Sciences*, **10** (6), 1183–1196.

Treloar, P. and C. Izatt, 1993. "Tectonics of the Himalayan collision between the Indian plate and the Afghan block: A synthesis". In: *Geological Society, London. Special Publications*.

Volant, P., F. Cotton and J.-C. Gariel, 1998. "Estimation of site response using the H/V method. Applicability and limits of this technique on Garner Valley downhole array dataset". In: *Proceedings of the 11th European conference on earthquake engineering*. Paris, France.

Wandrey, C., B. Law and H. Shah, 2004. Sembar Goru/Ghazij composite total petroleum system, Indus and Sulaiman-Kirthar geologic provinces, Pakistan and India. Tech. rep. Reston, VA, USA: US Department of the Interior, US Geological Survey.

Warnana, D., R. Ria and U. Widya, 2011. Application of microtremor HVSR method for assessing site effect in residual soil slope. *International Journal of Basic and Applied Sciences*, **11** (4), 73–78.

Wathelet, M., J.-L. Chatelain, C. Cornou, G. Di Giulio, B. Guillier, M. Ohrnberger and A. Savvaidis, 2020. Geopsy: A User-Friendly OpenSource Tool Set for Ambient Vibration Processing. *Seismological Research Letters*, **91**, 1878–1889.

Woolery, E. and R. Street, 2002. 3D near-surface soil response from H/V ambient-noise ratios. *Soil Dynamics and Earthquake Engineering*, **22** (9-12), 865–876.

Zaman, S. and P. Warnitchai, 2016. Topographically-Derived Near-Surface Shear Wave Velocity Map for Pakistan. *Journal of Earthquake and Tsunami*, **10** (2).

Zhao, J. *et al.*, 2006. Site Response Analysis of Soft Soil Sites Using a Shallow Shear Wave Velocity Profile. *Bulletin of the Seismological Society of America*, **96** (4), 1325–1337.

Appendix A. *Physiographic map*

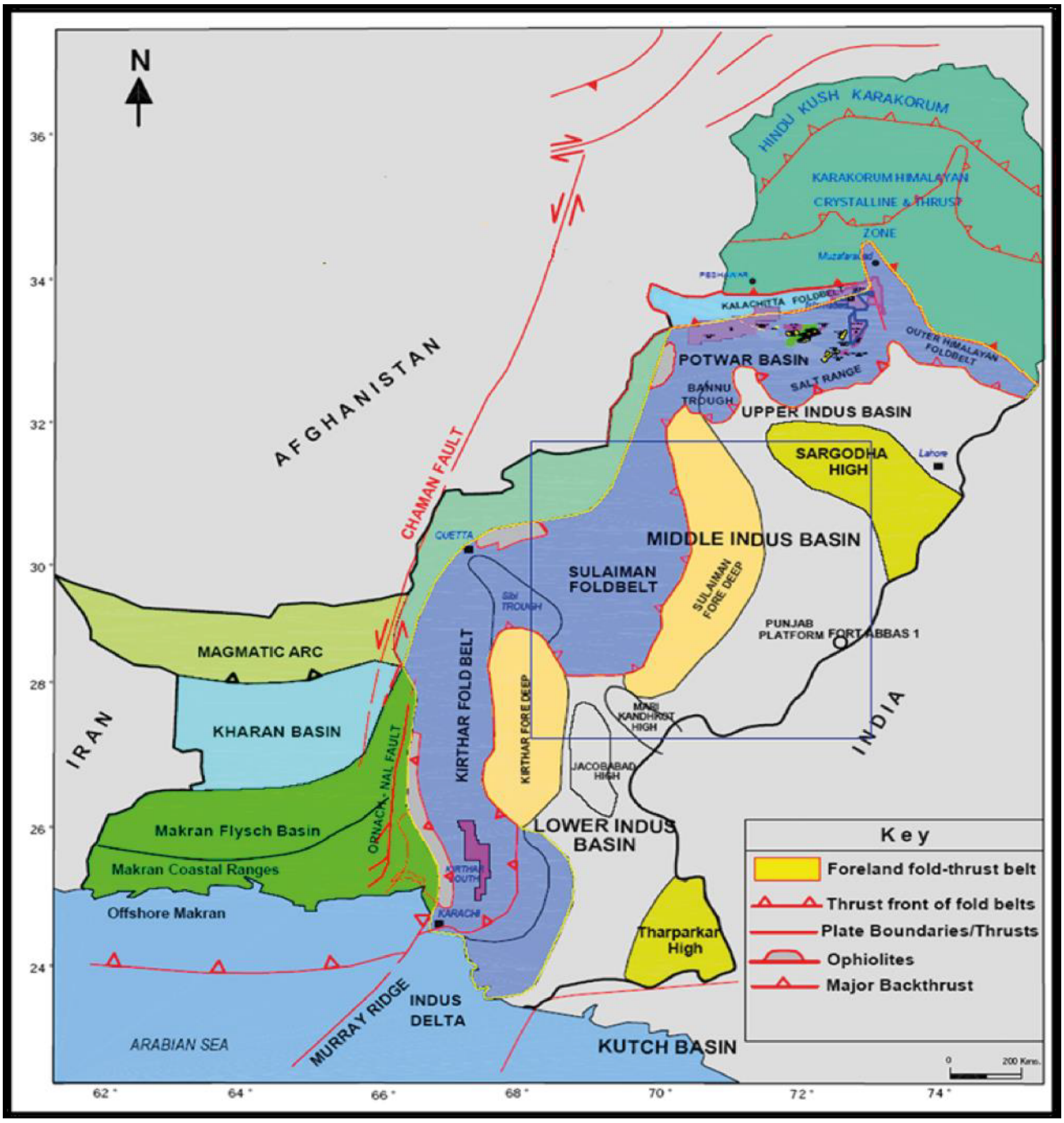

Fig. A.1: Map showing location of the Central Indus Basin where the study area is located. The remaining major physiographic units of Pakistan are also presented.